Archives of Biochemistry and Biophysics 673 (2019) 108079

Contents lists available at ScienceDirect

Archives of Biochemistry and Biophysics

journal homepage: www.elsevier.com/locate/yabbi

The multifunctional globin dehaloperoxidase strikes again: Simultaneous peroxidase and peroxygenase mechanisms in the oxidation of EPA pollutants

Talita Malewschik, Vesna de Serrano, Ashlyn H. McGuire, Reza A. Ghiladi*

Department of Chemistry, North Carolina State University, Raleigh, NC, 27695-8204, USA

ARTICLE INFO

Keywords:
Cresols
Dehaloperoxidase
Hemoglobin
Oxidation
Peroxidase
Peroxygenase

ABSTRACT

The multifunctional catalytic hemoglobin dehaloperoxidase (DHP) from the terebellid polychaete *Amphitrite ornata* was found to catalyze the H_2O_2-dependent oxidation of EPA Priority Pollutants (4-Me-*o*-cresol, 4-Cl-*m*-cresol and pentachlorophenol) and EPA Toxic Substances Control Act compounds (*o*-, *m*-, *p*-cresol and 4-Cl-*o*-cresol). Biochemical assays (HPLC/LC-MS) indicated formation of multiple oxidation products, including the corresponding catechol, 2-methylbenzoquinone (2-MeBq), and oligomers with varying degrees of oxidation and/or dehalogenation. Using 4-Br-*o*-cresol as a representative substrate, labeling studies with ^{18}O confirmed that the O-atom incorporated into the catechol was derived exclusively from H_2O_2, whereas the O-atom incorporated into 2-MeBq was from H_2O, consistent with this single substrate being oxidized by both peroxygenase and peroxidase mechanisms, respectively. Stopped-flow UV–visible spectroscopic studies strongly implicate a role for Compound I in the peroxygenase mechanism leading to catechol formation, and for Compounds I and ES in the peroxidase mechanism that yields the 2-MeBq product. The X-ray crystal structures of DHP bound with 4-F-*o*-cresol (1.42 Å; PDB 6ONG), 4-Cl-*o*-cresol (1.50 Å; PDB 6ONK), 4-Br-*o*-cresol (1.70 Å; PDB 6ONX), 4-NO_2-*o*-cresol (1.80 Å; PDB 6ONZ), *o*-cresol (1.60 Å; PDB 6OO1), *p*-cresol (2.10 Å; PDB 6OO6), 4-Me-*o*-cresol (1.35 Å; PDB 6ONR) and pentachlorophenol (1.80 Å; PDB 6OO8) revealed substrate binding sites in the distal pocket in close proximity to the heme cofactor, consistent with both oxidation mechanisms. The findings establish cresols as a new class of substrate for DHP, demonstrate that multiple oxidation mechanisms may exist for a given substrate, and provide further evidence that different substituents can serve as functional switches between the different activities performed by dehaloperoxidase. More broadly, the results demonstrate the complexities of marine pollution where both microbial and non-microbial systems may play significant roles in the biotransformations of EPA-classified pollutants, and further reinforces that heterocyclic compounds of anthropogenic origin should be considered as environmental stressors of infaunal organisms.

1. Introduction

A number of phenolic compounds have been classified as persistent organic pollutants (POPs) by the EPA and World Health Organization owing to their resistance to biodegradation [1,2]. As a consequence, bioaccumulation of POPs may cause severe and often long-lasting effects on the environment, spanning atmospheric, terrestrial, and marine systems [3,4]. Of similar concern, once released into the environment from anthropogenic sources, some phenolic compounds can undergo biotransformations owing to their similarity to naturally-produced compounds, forming secondary metabolites that can be even more toxic than the parent compound [5]. Relevant to the present study, examples of phenolic POPs include i) cresols (methylphenols), which are released into the environment mainly by industrial effluent or through the combustion of petroleum, coal, wood, and tobacco [6], and ii) pentachlorophenol, a common water contaminant that is primarily employed as a wood preservative and pesticide [7]. Due to their potential for significant environmental toxicity, adverse health effects after acute or chronic exposure, and long-term persistence leading to bioaccumulation, a range of phenol derivatives, including halophenols, nitrophenols, and cresols, have elevated threat levels and are either classified by the EPA as Priority Pollutants [1] or included in the Toxic Substances Control Act [2].

In light of their environmental toxicity, phenol biodegradation pathways have been the subject of numerous investigations. Microorganisms (e.g., bacteria and fungi) employ cresol isomers (*o*-, *m*-, *p*-cresol) as carbon sources, with initial oxidation of *p*-cresol to 4-methylcatechol and *o*-cresol to 3-methylcatechol and 2-

* Corresponding author. Department of Chemistry North Carolina State University Raleigh, NC, 27695, USA.
E-mail address: Reza_Ghiladi@ncsu.edu (R.A. Ghiladi).

https://doi.org/10.1016/j.abb.2019.108079
Received 16 May 2019; Received in revised form 19 August 2019; Accepted 20 August 2019
Available online 21 August 2019
0003-9861/

Abbreviations

ASU	Asymmetric Unit
2-MeBq	2-methyl-1 4-benzoquinone
4-Br-C	4-bromo-*o*-cresol
4-BP	4-bromophenol
4-Cl-C	4-chloro-*o*-cresol
4-F-C	4-fluoro-*o*-cresol
3-MC	3-methylcatechol
4-MC	4-methylcatechol
4-Me-C	4-methyl-*o*-cresol
4-NO_2-C	4-nitro-*o*-cresol
4-NP	4-nitrophenol
DMPO	5,5-dimethyl-1-pyrroline N-oxide
Compound I	two-electron oxidized heme cofactor compared to the ferric form, commonly as an Fe^{IV}=O porphyrin π-cation radical
Compound II	one-electron oxidized heme cofactor when compared to the ferric form, commonly as an Fe^{IV}=O or Fe^{IV}–OH
Compound ES	two-electron-oxidized state containing both a ferryl center [Fe^{IV}=O] and an amino acid (tryptophanyl or tyrosyl) radical, analogous to Compound ES in cytochrome *c* peroxidase
Compound RH	'Reversible Heme' state of dehaloperoxidase, formed from the decay of Compound ES in the absence of co-substrate
DHP	dehaloperoxidase
EI	electron ionization
EPA	Environmental Protection Agency
ESI	electrospray ionization
Hb	hemoglobin
HRP	horseradish peroxidase
HSM	horse skeletal muscle
Mb	myoglobin
PCP	pentachlorophenol
TBP	2,4,6-tribromophenol
TCP	2,4,6-trichlorophenol
TFA	trifluoroacetic acid
WT	wild-type

methylhydroquinone, followed by ring fission that leads to smaller products [8–11]. Additionally, *p*-cresol is oxidized by chloroperoxidase [12], manganese peroxidase [13], and polyphenol oxidase [14], and in the case of horseradish peroxidase (HRP) and ascorbate peroxidase (APX), common oxidation products include 2-dihydroxy-5,5-dimethylbiphenyl and tetrahydrodibenzofurane (Pummerer's quinone) [15,16]. Enzymes are also employed in the degradation of pentachlorophenol (PCP), including HRP and LiP [16], and PCP-degrading bacteria, such as *Sphingobium chlorophenolicum* and *Flavobacterium* sp., employ multiple enzymes for full mineralization of the chlorinated substrate [17,18]. Despite the insights afforded by these studies, the majority of them have focused on plant or microbial pathways, and comparatively fewer studies have addressed how infaunal organisms impact the fate of, or are themselves impacted by, persistent organic pollutants [19–22].

One such infaunal system that is potentially involved in the degradation of POPs and related xenobiotics is the multifunctional catalytic hemoglobin dehaloperoxidase (DHP) from *Amphitrite ornata* [23–29]. As a sediment-dwelling marine worm [30], *A. ornata* tolerates a diverse array of biogenically-produced organobromine compounds (secreted by other marine organisms as defense mechanisms [31]) by employing its hemoglobin as a detoxification enzyme. Named dehaloperoxidase [27,32], this O_2-transport protein [33,34] is capable of oxidizing a wide array of compounds, including mono, di- and trihalophenols [32], haloindoles [35], pyrroles [36], (halo)guaiacols [23] and nitrophenols [25], and also strongly binds azoles [24]. Substrate oxidation/degradation in DHP takes place via one of four canonical heme-based mechanisms: peroxidase [37–40], peroxygenase [25,35,36], oxidase [35], and oxygenase [41], with no crossover between these activities for a given class of substrate, i.e., halophenols, nitrocatechol, and haloguaiacols are oxidized solely via a peroxidase-based mechanism, and haloindoles, pyrrole, and nitrophenols are exclusively oxidized via a peroxygenase activity. To date, it is still not understood how DHP (as a multifunctional enzyme) controls for this activity differentiation given that all activities occur at a single site employing reactive intermediates (i.e., Compounds I [42,43], ES [37,38], and II [44]) that are commonly invoked in these four mechanisms [45–47]. Moreover, no mechanistic studies have explored the oxidation of cresols or pentachlorophenol by DHP as a model for infaunal organisms.

To address these questions, and in light of the need for further investigating biological systems of nonmicrobial origin in assessing the environmental fate and/or impact of phenolic compounds from the EPA Priority Pollutants and Toxic Substances Control Act lists, here we present structural, spectroscopic, and mechanistic studies describing the reactivity of cresols and pentachlorophenol with the multifunctional globin dehaloperoxidase, and establish cresols as a new class of substrate for DHP. We will show that unlike phenols/guaiacols (peroxidase, red box) and nitrophenols (peroxygenase, blue box), DHP is able to oxidize a given cresol substrate by both peroxidase and peroxygenase mechanisms (Fig. 1, purple box), and the ability to 'tune' DHP activity through the selection of the substrate (e.g., substituent effects [23,48,49]) will be discussed. The results here will demonstrate that DHP is a unique example of a multifunctional protein that challenges many of the assumptions behind the protein structure-function correlation that has been built from decades of study of monofunctional proteins, and provides us with a system for exploring how the substrate itself can have a significant influence in tuning the chemical reactivity exhibited by an enzyme.

2. Experimental

Materials. Ferric WT DHP B was expressed and purified as previously reported [38,50]. Oxyferrous DHP B was prepared by the aerobic addition of excess ascorbic acid to ferric DHP B, followed by desalting (PD-10 column) [44]. DHP concentration was determined spectrophotometrically using ε_{soret} = 116,400 M^{-1} cm^{-1} [38]. Horse skeletal muscle (HSM) myoglobin (ε_{soret} = 188,000 $M^{-1}cm^{-1}$ [51]), horseradish peroxidase (HRP) (ε_{soret} = 102,000 $M^{-1}cm^{-1}$ [52]) and mushroom tyrosinase from *Agaricus bisporus* (7164 U/mg; hydrated

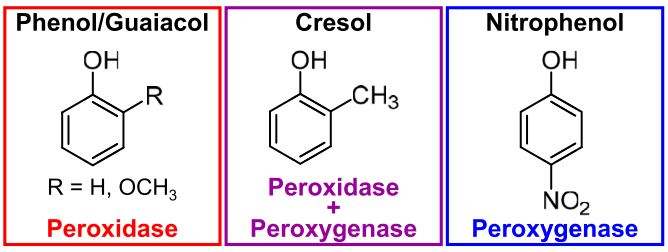

Fig. 1. Substituent effects modulate different oxidation mechanisms in DHP: peroxidase (red) and peroxygenase (blue), with cresols being oxidized by both mechanisms (purple). (For interpretation of the references to color in this figure legend, the reader is referred to the Web version of this article.)

using 100 mM KP_i at pH 7) were purchased from Sigma-Aldrich and used as received. Substrate stock solutions (10 mM) were prepared in methanol and stored at −80 °C. Solutions of H_2O_2 were prepared fresh daily in 100 mM KP_i (pH 7) and kept on ice until needed. Isotopically labeled $H_2{}^{18}O_2$ (90% ^{18}O-enriched) and $H_2{}^{18}O$ (98% ^{18}O-enriched) were purchased from Icon Isotopes (Summit, NJ). Acetonitrile (MeCN) was HPLC grade, and all other reagent-grade chemicals were purchased from VWR, Sigma-Aldrich or Fisher Scientific and used without further purification.

HPLC Reactivity Studies. Enzyme assays (250 μL total volume) were performed in triplicate in 100 mM KP_i at pH 7 (unless otherwise indicated) containing 5% MeOH at room temperature. A typical reaction was initiated by the addition of 500 μM H_2O_2 to a solution containing 10 μM enzyme and 500 μM substrate, and quenched after 5 min with an excess of catalase. Enzyme variants included ferric WT DHP B, ferric DHP B (Y28F/Y38F) [42], oxyferrous WT DHP B, HSM and HRP. Mechanistic probes were added prior to the addition of H_2O_2, including 500 μM 4-bromophenol (MeOH), 500 μM D-mannitol (KP_i), 100 mM 5,5-dimethyl-1-pyrroline N-oxide (DMPO; MeOH) or 10% v/v DMSO, and adjustments were made to ensure a final 5% MeOH concentration for all reactions except DMPO (10% MeOH final). A 200 μL aliquot of the reaction mixture was diluted 4-fold with 600 μL 100 mM KP_i at the reaction pH, and the diluted samples were analyzed using a Waters e2695 Separations Module coupled to a Waters 2998 photodiode array detector and equipped with a Thermo Fisher Scientific ODS Hypersil (150 mm × 4.6 mm) 5 μM particle size C_{18} column. Separation was performed using a linear gradient of binary solvents (solvent A, water + 0.1% TFA; solvent B, acetonitrile + 0.1% TFA). The elution consisted of the following conditions: (1.5 mL/min A:B) 95:5 to 5:95 linearly over 12 min, 5:95 isocratic for 2 min, 5:95 to 95:5 over 1 min, then isocratic for 3 min. Data analysis was performed using the Waters Empower software package.

Product Determination by LC-MS. The reactions were performed and quenched as described above with the exception that 5 mM KP_i (pH 7) buffer was employed. Analysis of the undiluted reaction (20 μL injection aliquot) was carried out using a Thermo Fisher Scientific Exactive Plus Orbitrap mass spectrometer employing a heated electrospray ionization (HESI) probe and equipped with a Thermo Hypersil Gold (50 × 2.1 mm, particle size 1.9 μm) C_4 column. The flow rate was set to 250 μL/min (solvent A, water + 0.1% formic acid; solvent B, acetonitrile + 0.1% formic acid) and the mass spectrometer was operated in both negative and positive ion modes to yield the $[M\text{-}H]^-$ and $[M+H]^+$ species, respectively. Spectra were collected while scanning from 100 to 1500 *m/z* and data analysis was performed using Thermo Xcalibur software. For the ^{18}O labeling studies, the reactions were performed for 10 min in the presence of DHP, substrate, and H_2O_2, where unlabeled H_2O_2 was replaced with $H_2{}^{18}O_2$, and/or the KP_i buffer was replaced with $H_2{}^{18}O$ to ensure > 90% of labeled ^{18}O was present.

Tyrosinase-Catalyzed Cresol Hydroxylation. The tyrosinase-catalyzed hydroxylations of 4-R-*o*-cresol (R = F, Cl, Br, NO_2), 4-Cl-*m*-cresol, *m*-cresol and *p*-cresol were performed per literature protocol with modifications [53–55]. Briefly, to a 1.5 dram glass vial was added neat cresol substrate (0.05 mmol), 1.5 equiv ascorbic acid (solid), 1.665 mL 100 mM KP_i buffer (pH 7) and 335 μL tyrosinase (7880 U/mL). The reaction was stirred open to air for 24 h at room temperature, quenched with 1 M HCl (1 mL), and subsequently analyzed by HPLC and LC-MS (negative ion mode) (*vide supra* for instrument and method information) prior to workup. The reaction mixture was then extracted with ethyl acetate (EtOAc; 2 x 2 mL), and the combined organic extracts were dried over sodium sulfate, filtered, and concentrated *in vacuo* to yield oils that ranged from colorless to dark brown. The crude product was redissolved in 150 μL EtOAc, followed by the addition of 100 μL pyridine, 100 μL hexamethyldisilazane and 50 μL of trimethylsilyl chloride (HMDS-TMCS, 2:1 v/v) [55]. This mixture was vigorously stirred for 30 min, allowed to stand for 5 min, and then centrifuged for 5 min at 10,000 rpm. The supernatant was analyzed on an Agilent 6890 Series GC System coupled to an Agilent 5973 Mass Selective Detector using a DB-5MS column (0.25 mm i.d. x 30 m, 0.25 μm film thickness). The method employed was as follows: isothermal at 100 °C for 2 min, a gradient of 10 °C/min to 280 °C, and maintained at 280 °C for 10 min [53]. The flow rate (He) was 15 mL/min, and the injection volume was 1 μL. Mass spectra were recorded with an electron beam of 70 eV, scanning from 50 to 550 *m/z*.

Binding studies. The substrate dissociation constants (K_d values) were determined in triplicate for ferric WT DHP B using a Cary 50 UV–vis spectrophotometer as per previously published protocols [35,56]. Against a reference spectrum of 50 μM ferric DHP B in 100 mM KP_i (pH 7) containing 5% MeOH, difference spectra were obtained for the addition of 0.5–150 equiv substrate to 50 μM DHP B while maintaining constant enzyme, buffer, and MeOH concentrations. Analysis of the visible region (450–700 nm) was performed using the ligand binding function in Grafit (Erithacus Software Ltd.).

Crystallization and Data Collection. Crystallization and data collection were performed using non-His-tagged ferric DHP B that was overexpressed and purified as per literature precedent [23,48–50]. The protein was crystallized from the ferric form using the hanging-drop vapor diffusion method. Crystals grew from 30 to 32% MPEG 2000, 0.2 M ammonium sulfate and 0.02 M sodium cacodylate (pH 6.5) by mixing protein at 10 mg/mL in 20 mM sodium cacodylate (pH 6.5) and crystallizing solution at 1:1, 1.5:1 or 2:1 of protein:reservoir solution. Crystals appeared after 3 days of incubation at 4 °C and were harvested after a growth period of one to two weeks. All the substrate-bound forms were obtained by overnight soaking of crystals in solutions containing 34% MPEG 2000, 0.2 M ammonium sulfate, and supplemented with varying concentrations of substrate (1–100 mM) dissolved in DMSO, with a final concentration of 5% DMSO in the soaking solution. The crystals were subsequently cryoprotected by dipping in soaking solution supplemented with 25% ethylene glycol, and flash cooled in liquid nitrogen before data collection. X-ray diffraction data were collected remotely at the SER-CAT ID22 and BM22 beamlines at the Advanced Photon Source, Argonne National Laboratories. The data sets were collected at 100 K, using a wavelength of 1.0 Å, employing a shutterless Rayonix MX300HS detector. The data were integrated and scaled with either iMosflm from CCP4 suite or HKL2000 program suite [57], molecular replacement was done with Phaser-MR [58] using 3IXF [50] coordinates as a search model, manual model building was performed in COOT [59], whereas refinement was carried out using REFMAC5 [60] in the CCP4 suite [61] and phenix.refine in the PHENIX suite of programs [62,63]. The final model was validated using COOT, MolProbity [64] and PDB_REDO [65].

Stopped-Flow UV–Visible Spectroscopic Studies. Optical spectra were recorded using a Bio-Logic SFM-400 triple-mixing stopped-flow instrument coupled to a rapid scanning (1.5 ms) diode array UV–vis spectrophotometer. The protein and H_2O_2 solutions were prepared in 100 mM KP_i (pH 7), and the substrates solutions were made in buffer containing 5% MeOH. Double-mixing experiments were performed using an aging line prior to the second mixing step to observe Compound I/ES/II reactivity with 10 equiv substrate, as follows: (i) Compound I was pre-formed from the reaction of ferric DHP B (Y28F/Y38F) [42] with 10 equiv H_2O_2 in an aging line for 85 ms prior to mixing with the substrate; (ii) Compound ES was pre-formed by reaction of ferric WT DHP B with 10 equiv of H_2O_2 in an aging line for 400 ms prior to mixing with the substrate [38]; (iii) Compound II was pre-formed from oxyferrous DHP B that was preincubated with 1 equiv TCP and then reacted with 10 equiv of H_2O_2 in an aging line for 2.75 s prior to mixing with the substrate [23,44]. Data were collected (900 scans total) over a three-time domain (1.5, 15, and 150 ms) observation period using the Bio-Kine 32 software package (Bio-Logic). All data were evaluated using the Specfit Global Analysis System software package (Spectrum Software Associates) and fit with SVD analysis as either one-step, two-species or two-step, three-species irreversible mechanisms, where applicable. For data that did not properly fit these

models, experimentally obtained spectra at selected time points detailed in the figure legends are shown. Data were baseline corrected using the Specfit autozero function.

3. Results and discussion

DHP-Catalyzed Substrate Reactivity with H_2O_2. The hydrogen peroxide-dependent reaction of ferric WT DHP B with the EPA Priority Pollutants and related substrates was monitored by HPLC, and the corresponding substrate conversion percentages (based upon substrate loss) are reported in Table 1. Reactions were initiated upon the addition of 500 μM H_2O_2 to a solution containing 10 μM ferric WT DHP B and 500 μM substrate, incubated at 25 °C for 5 min, and then quenched with catalase (as DHP does not possess any catalase activity). At pH 7, the substrate conversion ranged from a low value of 11% for pentachlorophenol to a high of ~67% for *p*-cresol. When repeated at pH 8, only modest changes (< 2-fold) were noted, likely attributable to protein-dependent pH effects given that the substrate pK_a values are below ~5 or above ~9.5 (pK_a values: *o*-cresol, 10.29 [66]; *m*-cresol, 10.26 [66]; *p*-cresol, 10.09 [66]; 4-Me-*o*-cresol, 10.60 [67]; 4-Cl-*o*-cresol, 9.71 [67]; 4-Cl-*m*-cresol, 9.55 [67]; pentachlorophenol, 4.70 [68]; 2,4-dinitro-*o*-cresol, 4.31 [69]). The order of oxidation of the cresol isomers was found as *o*-cresol ~ *m*-cresol < *p*-cresol, which mirrors their binding affinities (*vide infra*). An inverse relationship was observed between halogen size and enzyme reactivity for the 4-X-*o*-cresols halogen series (X = F, Cl, Br), with a 2-fold difference (F > Cl > Br) between the highest and lowest conversions. While an electronic effect cannot be ruled out, we note a significant difference in the substrate orientation within the active site for 4-F-*o*-cresol (51.8%) vs. 4-Cl-*o*-cresol (35.2%) and 4-Br-*o*-cresol (27.5%) as shown by X-ray crystallography (*vide infra*, Fig. S10). Finally, DHP B was also found to catalyze the oxidation of pentachlorophenol (11%), which now adds the fully substituted analog to the halophenol series 4-chlorophenol (inhibitor) [32,70], 2,4-dichlorophenol (substrate [32,71]) and 2,4,6-trichlorophenol (peroxidase substrate [32,38,72]). Finally, no reactivity was observed for 2,4-dinitro-*o*-cresol under any conditions examined, even when performed at pH 5 (data not shown), which is near its reported pK_a of 4.31. As DHP is able to catalyze the oxidation of 2,4-dinitrophenol (pK_a 4.07 [66]) at pH 5 and 6 [25], the lack of reactivity here with 2,4-dinitro-*o*-cresol is possible due to binding or electronic factors, and not pH-related. As expected, neither substrate turnover nor product formation were observed in the absence of H_2O_2 (non-oxidant control) or enzyme (non-enzymatic control) (data not shown).

As the native substrate scope of dehaloperoxidase is believed to be organobromine compounds [32], and as DHP B has been shown to oxidize brominated analogs of phenols [38], indoles [35], and guaiacols [23], mechanistic investigations were performed here with 4-Br-*o*-cresol (4-Br-C) as a representative substrate for the cresol family, the results of which are summarized in Table 2.

(i) pH *dependence:* a ~3-fold increase in substrate oxidation was observed as the reaction pH was increased from 5 (16.0%) to 8 (43.8%), with only a minor further increase at pH 9 (46.2%). This suggests that maximal activity occurs as the pH ≥ pK_a of the DHP metaquo acid–alkaline transition of 8.1 [73]. This is the opposite behavior as has been previously shown for DHP peroxygenase substrates 4-nitrophenol [25], pyrrole [36], and 5-Br-indole [35], where activity increased as the pH decreased.

(ii) *Enzyme variations:* the oxidation of 4-Br-*o*-cresol as catalyzed by oxyferrous DHP B (21.0%) was slightly attenuated compared to that of ferric DHP B (27.5%), but still demonstrated that the substrate oxidation reaction can be initiated from either the globin-active (Fe^{II}–O_2) or the peroxidase active (Fe^{III}) oxidation states, a result consistent with literature precedent [23,25,35,36,44,74,75]. Studies performed with DHP B (Y28F/Y38F), a mutant that yields Compound I as the initially-observed reactive intermediate rather than the Compound ES species observed in WT DHP B [42], showed only slightly lower substrate conversion (21.9%) compared to WT DHP. Whereas the canonical horseradish peroxidase (HRP) yielded virtually complete conversion (98.8%) of 4-Br-*o*-cresol, horse skeletal muscle myoglobin showed similar conversion (33.1%) compared to WT DHP B; in both cases, the product distributions were different from that observed for DHP (data not shown). Finally, DHP isoenzyme A, which differs from DHP B by only five amino acid substitutions [49,50], showed a higher conversion of 49.7% than the DHP B analog; the higher activity of isoenzyme A over that of B has only been observed previously with pyrrole (a peroxygenase substrate) [36].

(iii) *Mechanistic studies:* The addition of 4-bromophenol (K_d = 1.15 mM [70]), a known peroxidase and peroxygenase inhibitor [76,77], decreased substrate conversion by 1.7-fold, suggesting that 4-bromophenol has an inhibitory effect on 4-Br-*o*-cresol oxidation. When the reaction was performed in the presence of the known radical scavengers D-mannitol (26.1%) and DMPO (21.1%), no significant differences in substrate conversion or product distribution were noted, a result that suggests that solvent accessible radicals do not play a role in the oxidation of 4-Br-*o*-cresol. As a comparison, 4-Br-*o*-guaiacol, a peroxidase substrate, was similarly unaffected by DMPO, whereas this radical scavenger did inhibit 5-Br-*o*-guaiacol and 4-NO_2-*o*-guaiacol conversion, suggesting that these peroxidase substrates do proceed through diffusible radicals [23]. Finally, in the presence of DMSO, a slight increase (to 34.5%) in reactivity without change in product distribution was shown, which we attributed to the organic solvent facilitating access of the substrate to the hydrophobic binding pocket of DHP [78].

Taken together, the results obtained from the above enzymatic assays showed that dehaloperoxidase was able to catalyze the conversion of the EPA pollutants under physiological conditions, and establishes cresols as yet another class of phenolic substrate for DHP. These studies do not, however, provide definitive evidence for oxidation via either a peroxidase or peroxygenase-based mechanism, necessitating labeling studies (*vide infra*).

Identification of Reaction Products by HPLC and LC-MS. A representative chromatogram for each DHP B-catalyzed substrate oxidation reaction in the presence of H_2O_2 is found in Fig. 2, and the reaction mixtures were further analyzed by LC-MS. Under the conditions employed, multiple products were observed, and although identification of the exact chemical structures was not pursued, the products consisted of oligomers (up to n = 6) with varying degrees of oxidation; a list of the retention times, masses and chemical formulae obtained for the products (up to n = 3) can be found in Tables S1–S4. For the 4-X-cresol series (X = F, Cl, Br), dehalogenation products were also observed,

Table 1
DHP-catalyzed substrate oxidation studies.

Substrate	Conversion (%)	
DHP B WT Ferric	pH 7	pH 8
+ *o*-cresol	31.6 (± 6.2)	35.2 (± 2.9)
+ *p*-cresol	67.3 (± 3.6)	75.9 (± 3.5)
+ *m*-cresol	33.8 (± 2.2)	35.7 (± 3.0)
+ 4-Me-*o*-cresol	65.3 (± 6.7)	81.4 (± 11.5)
+ 4-F-*o*-cresol	51.8 (± 2.2)	53.7 (± 2.0)
+ 4-Cl-*o*-cresol	35.2 (± 3.7)	46.8 (± 5.7)
+ 4-Br-*o*-cresol	27.5 (± 3.5)	43.8 (± 4.3)
+ 4-NO_2-*o*-cresol	30.3 (± 3.0)	11.8 (± 2.3)
+ 2,4-dinitro-*o*-cresol	*n.d.*	*n.d.*
+ 4-Cl-*m*-cresol	35.4 (± 1.9)	23.1 (± 1.6)
+ pentachlorophenol	11.0 (± 2.1)	8.9 (± 1.3)

Reaction conditions: [ferric DHP B] = 10 μM, [substrate] = [H_2O_2] = 500 μM, 5% MeOH/100 mM KP_i (v/v) at pH 7 or 8, 25 °C, 5 min; *n.d.* = no reactivity detected.

Table 2
DHP-catalyzed oxidation of 4-Br-*o*-cresol as a function of enzyme variant, pH, and mechanistic probes.

Condition	Conversion (%)
pH *Studies*	
pH 5.0	16.0 (± 1.1)
pH 6.0	19.1 (± 1.0)
pH 7.0	27.5 (± 3.5)
- H_2O_2	*n. d.*
- enzyme	*n. d.*
pH 8.0	43.8 (± 4.3)
pH 9.0	46.2 (± 6.6)
Enzyme Variation	
DHP B Oxyferrous	21.0 (± 3.2)
DHP A Ferric	49.7 (± 1.4)
DHP B (Y28F/Y38F)	21.9 (± 1.5)
HRP	98.8 (± 0.2)
HSM Mb	33.1 (± 3.2)
Mechanistic Probes	
500 μM D-mannitol	26.1 (± 1.3)
10% DMSO	34.5 (± 2.3)
100 mM DMPO[a]	21.1 (± 5.0)
500 μM 4-bromophenol	15.0 (± 2.8)

Reaction conditions: [DHP] = 10 μM, [4-Br-*o*-cresol] = [H_2O_2] = 500 μM, 5% MeOH/100 mM KP_i (v/v), pH 7, 25 °C, 5 min; *n.d.* = no reactivity detected.
[a] reaction performed in 10% MeOH.

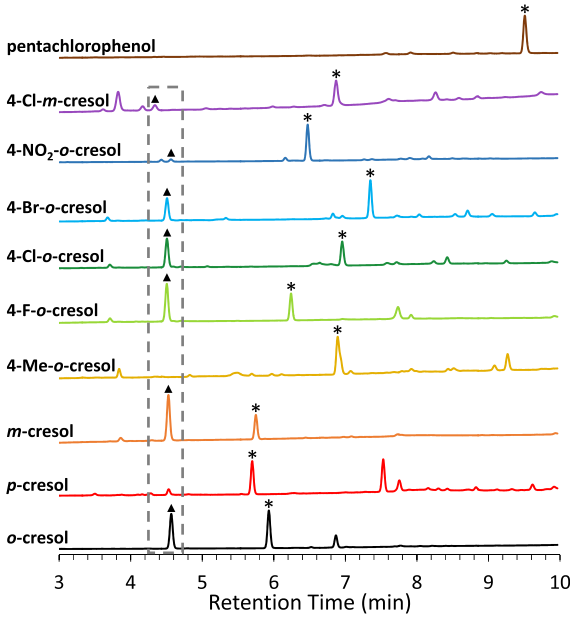

Fig. 2. HPLC chromatograms for the reaction of DHP B with the EPA priority pollutants and cresol derivatives in the presence of H_2O_2. Reaction conditions: 10 μM DHP B, 500 μM substrate, 500 μM H_2O_2, 5% MeOH/100 mM KP_i (v/v), pH 7, 25 °C. The reaction was quenched after 5 min with an excess of catalase. The 2-MeBq product is highlighted by the triangle with a t_R ~4.6 min. The asterisks denote the substrate. Reactions were monitored at 260 nm except pentachlorophenol (280 nm), and 4-X-*o*-cresol (X = F, Cl, Br; 265 nm).

consistent with previous studies employing 2,4,6-trihalophenols (yielding the corresponding 2,6-dihaloquinones [38]) and 4-X-guaiacols (forming oligomeric products) that also underwent oxidative dehalogenation chemistry [23].

For seven of the eleven substrates [*o*-cresol, *m*-cresol, 4-Cl-*m*-cresol and 4-R-*o*-cresol (R = F, Cl, Br, NO_2)] studied, a common oxidation product was observed. This product exhibited identical spectroscopic features (λ_{max} = 249 nm), retention time (t_R = 4.6 min), and mass (*m/z* 121.0, $[M\text{-}H]^-$; 123.0, $[M+H]^+$) that matched a commercial sample of 2-methyl-1,4-benzoquinone (2-MeBq; Fig. S1). On the basis of a calibration curve (Fig. S2), the amount of 2-MeBq was determined for each reaction (Table S5), and it was found that 2-MeBq formation varied up to 150-fold (0.2–28.9 μM) at pH 7, but only ~5-fold at pH 8 (5.2–27.8 μM, pH 8). The formation of the 2-MeBq indicates dehalogenation (-HX, X = F, Cl, Br) and loss of nitrite (HNO_2), and although no attempts were made to identify the leaving groups, stopped-flow UV/visible spectroscopic studies suggest that the halogen ions could serve as ligands to the heme-Fe, forming Fe-X adducts (*vide infra*). No 2-MeBq product was observed in the reactions with *p*-cresol, 4-Me-*o*-cresol and pentachlorophenol, and the yield of 2-MeBq product was unaffected when 100 mM DMPO was included in the 4-Br-*o*-cresol reaction. Quinone product formation has precedent for the DHP-catalyzed oxidative dehalogenation of 2,4,6-trihalophenol (X = F, Cl, Br) yielding the corresponding 2,6-dihaloquinone [32], and 4-X-*o*-guaiacol (X = F, Cl, Br) yielding 2-methoxybenzoquinone (2-MeOBQ) [23], with both reactions proceeding via a peroxidase-based mechanism. Formation of these quinone products has been previously linked to a product-driven reduction [23,38] owing to the unusually high redox potential of DHP [79], thereby providing a resolution to the 'dehaloperoxidase paradox' [80] wherein the product of its peroxidase activity (with an Fe^{III} resting state) reduces DHP back to the ferrous oxidation state, thereby rescuing its oxygen-transport function.

Identification of a Catechol Reaction Product. With the exception of pentachlorophenol, each substrate oxidation reaction exhibited a product that corresponded to the incorporation of an O-atom into the substrate (monomer + 1 O; Tables S1–S3). To determine if these products could be specifically ascribed to catechol formation, authentic samples of the corresponding catechol, either from commercial sources or prepared enzymatically (see Supporting Information), were employed as follows:

(i) 4-methylcatechol (4-MC) was found to have the same characteristic retention time (t_R = 4.4 min), UV–visible spectrum (λ_{max} = 225 nm) and mass (*m/z* $[M\text{-}H]^-$ = 123) as one of the oxidation products of *p*-cresol in the HPLC chromatogram (Fig. S3), confirming the formation of 4-MC during the DHP-catalyzed oxidation of *p*-cresol.
(ii) 3-methylcatechol (3-MC) showed a retention time of 4.7 min (λ_{max} = 225 nm), however, when compared to the *o*-cresol chromatogram, no peak with the same retention time and spectroscopic profile was observed (data not shown), despite the presence of the corresponding mass (*m/z* $[M\text{-}H]^-$ = 123; Table S1) being observed by LC-MS for the oxidation of *o*-cresol. This suggests that the 3-methylcatechol product is present at very small concentrations in the reaction mixture.
(iii) As they were not commercially available, the catechol derivatives for 4-R-*o*-cresol (R = F, Cl, Br, NO_2), 4-Cl-*m*-cresol, and *m*-cresol were synthesized enzymatically employing tyrosinase following literature protocols [53–55], and their characterization by GC-MS, LC-MS and HPLC can be found in the Supporting Information (Figs. S4–S6). As shown in Figs. S5 and S6, catechol products were identified by their retention time and UV–visible spectrum in the DHP-catalyzed oxidation of 4-F-*o*-cresol, 4-NO_2-*o*-cresol, 4-Cl-*m*-cresol and *m*-cresol.

Altogether, O-atom incorporation for five cresol substrates was confirmed from authentic samples that were either obtained commercially or enzymatically, with hydroxylation of the remaining cresol substrates (excluding pentachlorophenol) indicated by the LC-MS data. These results suggest the possibility of peroxygenase activity with the cresol substrates, an activity that has been observed for DHP with pyrrole [36], 5-Br-indole [35], and nitrophenol [25] substrates, but not with halophenol nor haloguaiacol substrates, these latter two being oxidized via a peroxidase activity.

Labeled Oxygen Studies. In order to determine the origin of the O-

atom that was incorporated in the *para* (2-MeBq) and *ortho* (catechol) positions of the oxidation products, labeling studies with 4-Br-*o*-cresol (as a representative substrate) were conducted employing $H_2{}^{18}O$ and $H_2{}^{18}O_2$ (98% and 90% enriched, respectively), and the results were subsequently analyzed by LC-MS in positive and negative modes to yield the $[M+H]^+$ and $[M\text{-}H]^-$ species, respectively. The background-subtracted total ion chromatograms (TICs) are shown in Figs. 3 and 4. The data were obtained in both ionization modes as the catechol (5-bromo-3-methyl-1,2-benzenediol) and 2-methyl-1,4-benzoquinone (2-MeBq) products could only be observed in negative and positive ion modes, respectively.

2-Me-1,4-benzoquinone (2-MeBq): In the presence of unlabeled H_2O and labeled $H_2{}^{18}O_2$, no increase in mass for 2-MeBq was observed [*m/z*: 123.08, 100% (Fig. 3C)] when compared with the results obtained in the absence of an ^{18}O source (Fig. 3A). The presence of $H_2{}^{18}O$ and unlabeled H_2O_2, however, resulted in an increase of 2 and 4 Da in the 2-MeBq mass [*m/z*: 123.08, 10.9%; 125.05, 38.1%; 127.05, 51.0% (Fig. 3B)], suggesting incorporation of labeled oxygen from water, with further scrambling from solvent occurring to account for the second labeled oxygen in 2-MeBq. The results obtained for the reaction employing both labeled $H_2{}^{18}O$ and $H_2{}^{18}O_2$ [*m/z* 123.05, 16.2%; 125.05, 36.7%; 127.05, 47.1% (Fig. 3D)] were virtually identical to those of the $H_2{}^{18}O/H_2O_2$ reaction, providing strong evidence for O-atom incorporation derived exclusively from water (and not from hydrogen peroxide), and consistent with a peroxidase mechanism for cresol oxidation by DHP yielding 2-MeBq. Additionally, the oligomeric products were observed to contain ^{18}O only in reactions that contained labeled water (data not shown).

5-Br-3-Me-1,2-benzenediol: In the presence of labeled $H_2{}^{18}O$ and unlabeled H_2O_2, no increase in mass for the catechol [*m/z*: 200.96 (^{79}Br), 48.3%; 202.96 (^{81}Br), 51.6% (Fig. 4B)] was observed when compared with the results obtained in the absence of an ^{18}O source (Fig. 4A). However, in the presence of unlabeled H_2O and labeled $H_2{}^{18}O_2$ there was an increase of 2 Da in the catechol mass [*m/z*: 200.96, 7.2%; 202.96 (^{79}Br), 48.6%; 204.96 (^{81}Br), 44.2% (Fig. 4C)], which strongly suggests that the origin of the O-atom incorporated into the catechol product was derived from hydrogen peroxide. Further, the results obtained for the reaction employing both labeled $H_2{}^{18}O$ and $H_2{}^{18}O_2$ [*m/z*: 200.96, 1.8%; 202.96 (^{79}Br), 48.3%; 204.96 (^{81}Br), 49.9% (Fig. 4D)] were virtually identical to those of the $H_2O/H_2{}^{18}O_2$ reaction, and provides unequivocal evidence that the oxygen atom was derived exclusively from hydrogen peroxide, with no incorporation of oxygen from water, and consistent with a peroxygenase mechanism for cresol oxidation by DHP for catechol formation.

Substrate Binding Studies. While the titration of substrates (0.5–150 equiv; Figs. S7–S9) to ferric WT DHP B in 100 mM KP_i/5% MeOH (v/v) showed no significant changes to the Soret band (data not shown), the Q-band region (450–700 nm) showed well-behaved optical difference spectra, thereby allowing for the determination of the apparent substrate binding constant (K_d). On a whole, the EPA pollutants exhibited a stronger binding affinity to DHP B when compared to the corresponding substituted guaiacols [23], halophenols [70] and pyrroles [36], but relatively similar K_d values as the nitrophenol [25], haloindole [35] and azole [24] substrates (Table 3). Across the halogenated 4-X-*o*-cresol series, a trend of increasing binding affinity with increasing halogen size was noted, H < F < Cl < Br. This same trend has been previously reported for the 4-X-*o*-guaiacol [23] and 5-X-indole [35] series, and is attributed to the Xe1 binding pocket in DHP B (hydrophobic cavity surrounded by amino acids L100, F21, F24, F35 and V59) having a higher affinity for larger halogen atoms, as deduced from crystallographic studies of 4-X-phenol binding to DHP [81]. The binding affinity of 4-bromophenol (K_d = 1.15 mM [70]), is 13-fold weaker than the affinity of 4-Br-*o*-cresol (K_d = 0.086 mM), which likely explains why the reactivity of this substrate was only partially affected (decreased 1.7-fold) in the presence of the inhibitor (Table 2).

X-Ray Crystallographic Studies. The structures of DHP B in complex with pentachlorophenol, 4-R-*o*-cresol (R = H, F, Cl, Br, Me, NO_2) and *p*-cresol were determined by X-ray crystallography to near atomic resolution (1.35–2.1 Å). Selected distances for substrate interactions and occupancy in the distal pocket can be found in Table 4, and the crystallographic data collection, processing, and structure refinement results are given in Table S6. The protein crystallized in the space group $P2_12_12_1$ with two molecules in the asymmetric unit (protomer A and protomer B), as was reported in our previous studies [23,25,48,49,71]. The substrates were found to bind in the distal heme cavity, positioned ~3.2–5 Å above the heme moiety, with the phenol ring substituents directing substrate orientation in the hydrophobic binding cavity above the heme (Fig. 5).

For the halogenated cresols 4-X-*o*-cresols (X = F, Cl, Br; Fig. 5A–C),

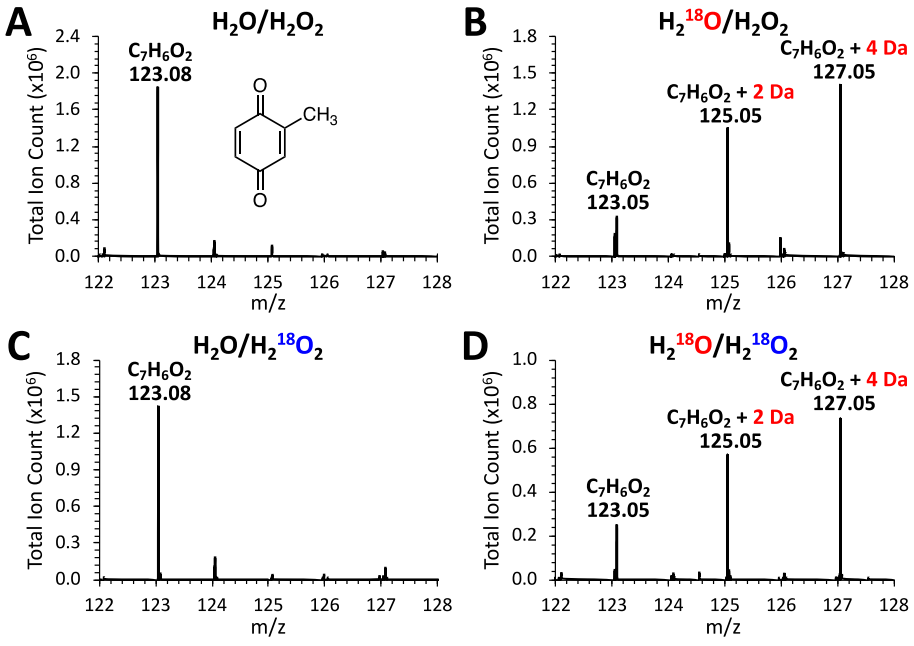

Fig. 3. ESI-MS total ion chromatograms obtained in positive ion mode for the 2-methylbenzoquinone (2-MeBq) product observed in the reaction of 4-BrC with DHP B: (A) H_2O/H_2O_2, (B) $H_2{}^{18}O/H_2O_2$, (C) $H_2O/H_2{}^{18}O_2$, and (D) $H_2{}^{18}O/H_2{}^{18}O_2$. Reactions conditions: 10 μM DHP B, 500 μM 4-Br-*o*-cresol, 500 μM H_2O_2, 5% MeOH/5 mM KP_i (v/v), pH 7, 25 °C, 10 min.

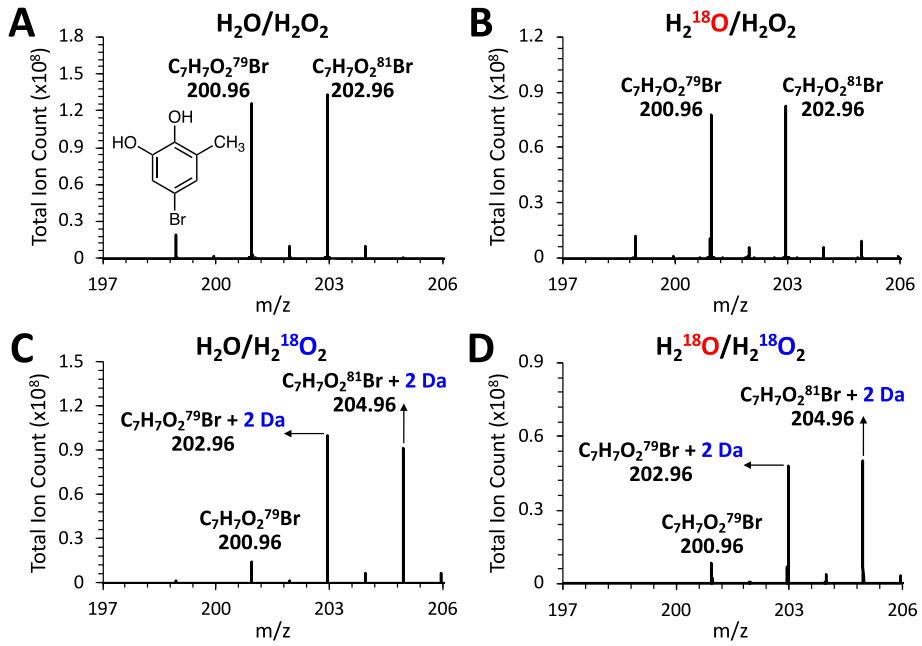

Fig. 4. ESI-MS total ion chromatograms obtained in negative ion mode for the 5-Br-3-Me-1,2-benzenediol (catechol) product observed in the reaction of 4-BrC with DHP B: (A) H_2O/H_2O_2, (B) $H_2{}^{18}O/H_2O_2$, (C) $H_2O/H_2{}^{18}O_2$, and (D) $H_2{}^{18}O/H_2{}^{18}O_2$. Reactions conditions: 10 μM DHP B, 500 μM 4-Br-*o*-cresol, 500 μM H_2O_2, 5% MeOH/5 mM KP_i (v/v), pH 7, 25 °C, 10 min.

Table 3
K_d Values for Substrate Binding to Ferric WT DHP B at pH 7.

Substrate	K_d (μM)	Ref
EPA Pollutants		
o-Cresol	4594 (± 393)	[a]
p-Cresol	2682 (± 381)	[a]
m-Cresol	6721 (± 582)	[a]
4-Me-*o*-cresol	309 (± 26)	[a]
4-F-*o*-cresol	2970 (± 391)	[a]
4-Cl-*o*-cresol	130 (± 4)	[a]
4-Br-*o*-cresol	86 (± 14)	[a]
4-NO_2-*o*-cresol	155 (± 5)	[a]
4-Cl-*m*-cresol	629 (± 36)	[a]
Pentachlorophenol	79 (± 9)	[a]
Substituted Guaiacols		
o-guaiacol	14712 (± 714)	[23]
4-Me-*o*-guaiacol	1433 (± 97)	[23]
4-F-*o*-guaiacol	2438 (± 207)	[23]
4-Cl-*o*-guaiacol	493 (± 53)	[23]
4-Br-*o*-guaiacol	374 (± 42)	[23]
4-NO_2-*o*-guaiacol	1341 (± 26)	[23]
Phenol		
4-bromophenol	1150	[70]
4-nitrophenol	262 (± 23)	[25]
Indole		
5-Cl-indole	317 (± 23)	[35]
5-Br-indole	150 (± 10)	[35]
5-I-indole	62 (± 10)	[35]
Azole		
Imidazole	52 (± 2)	[24]
Benzotriazole	82 (± 2)	[24]
Benzimidazole	110 (± 8)	[24]

[a] This work.

bulky atoms such as Br were found to bind deeper in the hydrophobic region, closer to residues L100 and F60 in the hydrophobic cavity above the α heme edge (Xe1 hydrophobic binding pocket), which is in accordance with previously published structures [81]. When compared with 4-Br-*o*-guaiacol (PDB 6CKE [23]), the halogen atoms of 4-Cl/Br-*o*-cresol superimpose exactly with the *p*-Br substituent of the guaiacol (Fig. S10A) in the Xe1 hydrophobic cavity, while the *o*-OMe group coincides with the *o*-Me group. Additionally for the 4-Cl/Br-*o*-cresol structures, H55 was found positioned inside the heme cavity, which enables hydrogen bonding interactions with the hydroxyl group of the substrate (Fig. 5B and C). The overall strong affinity of these two substrates with the enzyme (4-Cl-*o*-cresol, K_d = 130 μM; 4-Br-*o*-cresol, K_d = 86 μM; Table 3) is a reflection of these interactions, with an additional stabilization arising from π-stacking of the substrate aromatic ring with F21. By contrast, 4-F-*o*-cresol was found to bind closer to the heme γ edge and the heme propionate D due to hydrogen bonding interactions of the hydroxyl group with both T56 and Y38, mediated by a water molecule (Fig. 5A), which could reflect in its weaker binding affinity (K_d = 2970 μM) compared to 4-Cl-*o*-cresol and 4-Br-*o*-cresol. Two distinct conformations were observed for 4-F-*o*-cresol and 4-Cl-*o*-cresol on protomers B and A, respectively (Figs. S11A–B), which affected whether H55 was in the open or closed conformation, as well as substrate occupancy (4-F-*o*-cresol: A 55%, B, 20%; 4-Cl-*o*-cresol: A 58% and 20%).

The cresol substrates with less bulky substituents in the *para* position were found to bind in a similar position as 4-F-*o*-cresol. Two conformations were observed for *o*-cresol (protomer A) and 4-Me-*o*-cresol, where the hydroxyl group is either facing up towards Y38 or facing down towards the heme. When facing down, *o*-cresol (Fig. 5E) has a hydrogen bonding interaction to a water molecule positioned 3.3 Å away from the iron center, and when facing up the hydroxyl group of *o*-cresol interacts with propionate D and Y38. Additionally, *o*-cresol showed the presence of only one substrate conformation in protomer B (Fig. S11C), oriented such to be able to hydrogen bond with Y38 and heme propionate D. The hydroxyl group of 4-Me-*o*-cresol (Fig. 5G) has two different hydrogen bonding interactions when facing up: i) an interaction with T56 and, ii) an interaction with propionate D and Y38 mediated by a water molecule, which together can account for relatively strong affinity of this substrate with the protein (K_d = 309 μM). The *p*-cresol (Fig. 5F) isomer, for which only one conformation was observed in both chains and with the methyl group facing towards the Xe1 hydrophobic cavity, shows H-bonding interactions of the hydroxyl group with the heme propionate D and Y38, which together correlate to a stronger binding affinity compared to *o*-cresol (*o*-cresol, K_d = 4594 μM vs. *p*-cresol, K_d = 2682 μM). When comparing the structures of *o*-cresol, *p*-cresol, and 4-Me-*o*-cresol to 4-MeO-*o*-guaiacol (PDB 6CH6 [23]), the 4-MeO-*o*-guaiacol binding is significantly different (Fig. S10B), likely due to the bulkier -OMe vs -Me group, which

Table 4
Selected distances (angstroms) for DHP B-EPA pollutants complex (protomer A).

	4-F-*o*-cresol	4-Cl-*o*-cresol[a]	4-Br-*o*-cresol[b]	4-NO_2-*o*-cresol	*o*-cresol[c]	*p*-cresol	4-Me-*o*-cresol[c]	Pentachlorophenol[c]
PDB Entry	6ONG	6ONK	6ONX	6ONZ	6OO1	6OO6	6ONR	6OO8
Substrate occupancy	80%	100%	70%	70%	A: 50% B: 20%	100%	A: 20%, B: 60%	A: 40%, B: 15%
H55 N^{ε} … -OH (substrate)	^{ext}7.3	2.7	^{int}2.4/^{ext}9.1	^{ext}5.9	$5.7^{A}/7.1^{B}$	5.7	$7.3^{A}/7.0^{B}$	$5.1^{A}/5.2^{B}$
H55 N^{δ} … OH (substrate)	^{ext}5.6	4.7	^{int}4.4/^{ext}8.9	^{ext}4.1	$3.8^{A}/5.0^{B}$	3.7	$5.4^{A}/4.9^{B}$	$4.9^{A}/5.3^{B}$
F21 C^{ζ} … C^{1} (substrate)	3.5	3.8	3.8	3.8	$4.5^{A}/3.7^{B}$	4.4	4.0	$4.4^{A}/4.5^{B}$
F21 C^{γ} … C^{4} (substrate)	4.6	4.0	4.0	3.8	$3.8^{A}/2.9^{B}$	4.8	3.1	$4.7^{A}/5.9^{B}$
Fe···OH (substrate)	6.9	4.9	4.8	7.3	$7.3^{A}/4.5^{B}$	7.1	$7.0^{A}/4.9^{B}$	$7.5^{A}/7.6^{B}$
Fe···C^{o}–^{CH3} (substrate)	4.7	5.1	5.1	4.6	$4.8^{A}/7.3^{B}$	4.4	$4.9^{A}/7.3^{B}$	–
Fe … X[d] (substrate)	4.8	8.6	8.7	5.4^{N}, 5.1^{O1}, 6.2^{O2}	–	–	$4.8^{A}/7.3^{B}$	$3.7^{A}/2.2^{B}$
Fe···H55 N^{ε}	^{ext}10.3	5.9	^{int}5.6/^{ext}9.8	^{ext}10.0	10.2	10.3	10.4	^{int}4.7/^{ext}9.4
Fe···H55 N^{δ}	^{ext}8.5	6.4	^{int}6.0/^{ext}10.0	^{ext}8.1	8.3	8.5	8.5	^{int}6.2/^{ext}9.7
Fe···H89 N^{ε}	2.1	2.1	2.1	2.2	2.2	2.2	2.1	2.2
Fe to pyrrole N plane	0.274	0.254	0.188	0.175	0.193	0.158	0.262	0.0942

[a] For 4-Cl-C, numbers shown for protomer B.
[b] For 4-Br-C, H55 was found to be both in the interior and exterior conformations, designated as interior (int) or exterior (ext).
[c] The alternate substrate conformations are denoted with superscripts A and B.
[d] X refers to the substituent on *para* position.

nicely illustrates how subtle differences in the size of a substituent can lead to a significant change in how that substrate binds to DHP, an effect that can be used to 'tune' the activity of DHP between peroxidase and peroxygenase mechanisms [23,48].

The binding of 4-NO_2-*o*-cresol is similar to that observed for *p*-cresol (Fig. 5D), where the hydroxyl group is involved in hydrogen bonding interactions with both propionate D of the heme and Y38, and the nitro group is facing towards the Xe1 hydrophobic cavity. When compared to the structures of DHP B complex with 4-NO_2-phenol (PDB 5CHQ [25]), 4-NO_2-catechol (PDB 5CHR [25]) and 4-NO_2-*o*-guaiacol (PDB 6CH5 [23]) (Fig. S10C), the 4-NO_2-*o*-cresol binding position is nearly identical to both 4-NO_2-phenol and 4-NO_2-catechol, although it is displaced higher up relative to the heme plane in order to avoid a steric clash of the methyl group with the heme plane. As was found with 4-MeO-*o*-guaiacol, 4-NO_2-*o*-guaiacol binding was significantly different from that of the cresol analog due to the bulkier -OMe group.

The structure of DHP B in complex with pentachlorophenol (K_d = 79 μM) was determined using chlorine anomalous scattering (see Supporting Information). Pentachlorophenol was found close to the γ and δ heme edges, and in two conformations at nearly right angles to each other: one parallel (15% occupancy) and the other perpendicular (40% occupancy) to the heme cofactor (Fig. 5H). The parallel conformation extends towards the groove between residues F21 and F35, with H-bonding interactions between the hydroxyl group, Y38 and heme propionate D, whereas the perpendicular conformation enables π-stacking with F21 and H-bonding between the hydroxyl group, T56 and Y38. Not surprisingly, this perpendicular conformation is nearly identical in orientation and position as the peroxidase substrate 2,4,6-trichlorophenol (TCP; PDB 4KMW [72]), but also to the inhibitor 4-chlorophenol (PDB 3LB3 [70]) (Fig. S10D). Both perpendicular and parallel conformations showed slightly shifted positions in chain B (Fig. S11D), where the hydroxyl group for both was found to be interacting with Y38 and heme propionate D.

Overall, three distinct groups of H-bonding interactions for the hydroxyl group of the cresol substrate were noted (Fig. S10E): i) H-bonding to T56/Y38 mediated by a water molecule, as was observed for 4-F-*o*-cresol and 4-Me-*o*-cresol, which were also two of the most reactive substrates (Table 1); ii) H-bonding directly to Y38 and the heme propionate D, observed for *o*-, *p*- and 4-NO_2-*o*-cresol; and iii) H-bonding to H55 oriented inside the distal heme cavity, noted for 4-Cl-*o*-cresol

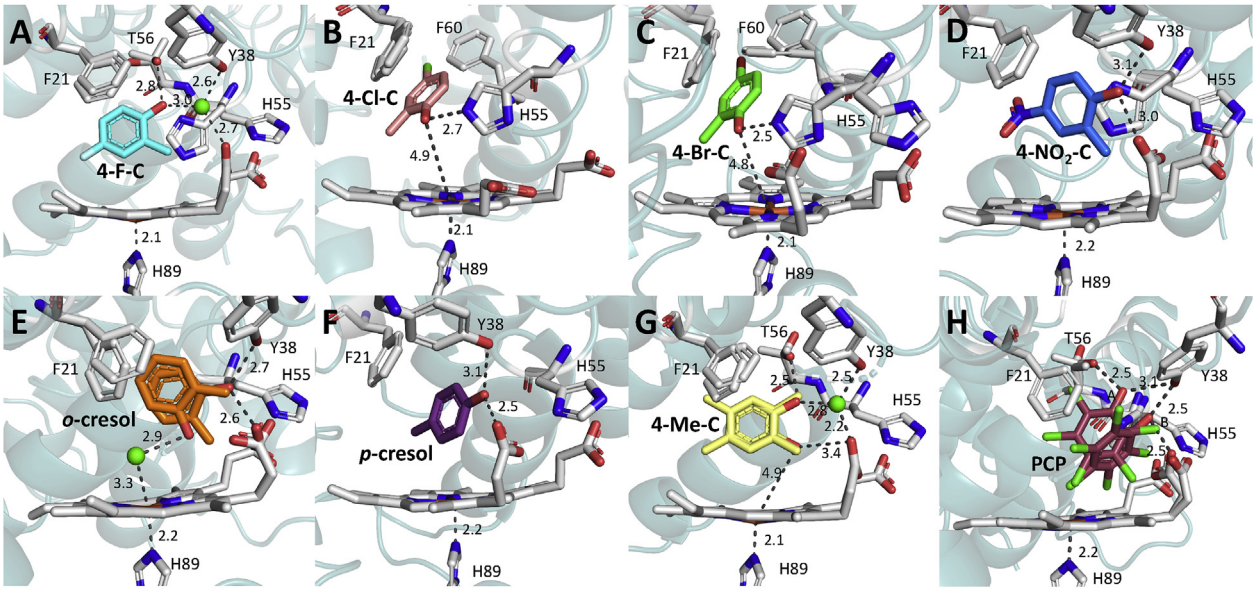

Fig. 5. X-ray crystal structures obtained for DHP B in complex with (A) 4-F-*o*-cresol [cyan, PDB 6ONG], (B) 4-Cl-*o*-cresol [pink, PDB 6ONK], (C) 4-Br-*o*-cresol [green, PDB 6ONX], (D) 4-NO_2-*o*-cresol [blue, PDB 6ONZ], (E) *o*-cresol [orange, PDB 6OO1], (F) *p*-cresol [purple, PDB 6OO6], (G) 4-Me-*o*-cresol [yellow, PDB 6ONR], and (H) pentachlorophenol [burgundy, PDB 6OO8]. Panels provide atomic distances and interactions between the substrate and amino acids and/or heme macrocycle.

and 4-Br-*o*-cresol, i.e., the substrates that bind deeper in the hydrophobic region of the distal pocket.

Stopped-Flow UV–Visible Spectroscopic Studies. As a representative substrate, the oxidation of 4-Br-*o*-cresol as catalyzed by DHP B was investigated using stopped-flow UV–Visible spectroscopy employing single and double-mixing methodologies (Fig. 6). Studies were performed with H_2O_2-activated DHP, preformed as Compound I [42,43], Compound ES [37,38], or Compound II [44]. As the kinetics were difficult to deconvolute at higher substrate concentrations owing to competing oxidation mechanisms and products formed therefrom, the studies presented here were limited to 10 equiv 4-Br-*o*-cresol, and the data were fit as one-step/two species or two-step/three species irreversible mechanisms where possible, or alternatively displayed as experimentally obtained spectra at selected time points.

Compound I Reactivity: Pre-formed in an aging line for 85 ms from an initial mixing step of ferric DHP B (Y28F/Y38F) with 10 equiv H_2O_2 [42], Compound I [406 (Soret), 528, 645 nm] [29] was reacted with 10 equiv 4-Br-*o*-cresol at pH 7 (Fig. 6A). The first spectrum had features that matched that of ferric DHP B (Y28F/Y38F) [406 (Soret), 509, and 636 nm; black, t = 0 s], suggesting that Compound I was rapidly reduced by the substrate within the mixing time (1.5 ms) of the stopped-flow apparatus, an observation that has been noted previously for other DHP substrates, including 5-Br-indole [35], 4-nitrophenol [25], pyrrole [36], and 4-Br-guaiacol [23]. Given the relatively slow reduction of Compound II by 4-Br-*o*-cresol (*vide infra*), the lack of an observable one-electron oxidized intermediate (i.e., DHP Compound II) suggests a single two-electron oxidation of 4-Br-*o*-cresol as opposed to two consecutive one-electron processes, a supposition that is supported by the lack of an effect by the radical scavenger DMPO (no diffusible radical formation). The ferric spectrum slowly converted to a final species [405 (Soret), 498, 605 nm; blue, t = 10 s] whose spectral features have been ascribed to an Fe–Br adduct [76], and suggests that the oxidative dehalogenation of 4-Br-*o*-cresol yields bromide that ultimately binds to the ferric enzyme. As opposed to the reaction chemistry with 2,4,6-tribromophenol, TCP, and 4-Br-guaiacol, this is the first time the DHP Fe-X adduct has been observed during Compound I-catalyzed substrate oxidation [23,42]. At longer observation times (500 s), the Fe–Br adduct converted to a species whose spectral features matched those of Compound RH, an inactivated form of DHP B (data not shown) [37,38,82].

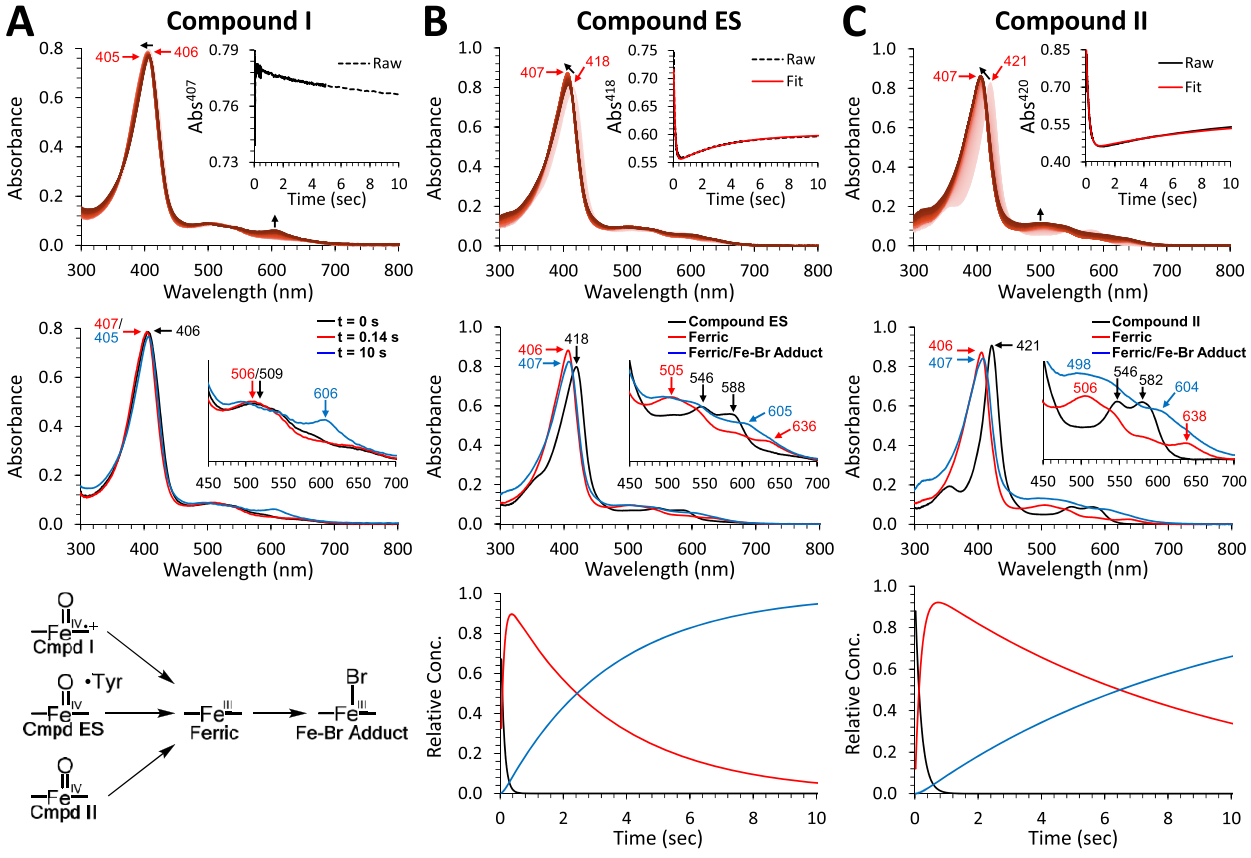

Fig. 6. Kinetic data obtained by optical spectroscopy for the reaction of H_2O_2-activated DHP B with 4-Br-*o*-cresol at pH 7. **A) DHP B (Y28F/Y38F)/Compound I:** *top panel*, stopped-flow UV–visible spectra of the double-mixing reaction of preformed Compound I (10 μM) with a 10-fold excess of 4-Br-*o*-cresol (614 scans over 10 s); inset: the single-wavelength (407 nm) dependence on time obtained from the raw data. *Bottom panel*, experimentally obtained spectra for Compound I reacted with 4-Br-*o*-cresol (black, t = 0 s), its reduction to the ferric enzyme (red, t = 0.14 s) and the formation of the Fe–Br adduct (blue, t = 10 s). **B) Ferric WT DHP B/Compound ES:** *top panel*, stopped-flow UV–visible spectra of the double-mixing reaction of preformed Compound ES with a 10-fold excess of 4-Br-*o*-cresol (610 scans over 10 s); inset: the single-wavelength (418 nm) dependence on time obtained from the raw spectra and its fit with a superposition of the calculated spectral components. *Middle panel*, the calculated spectra of the three reaction components derived from SVD analysis: Compound ES (black), ferric DHP B (red) and the Fe–Br adduct (blue). *Bottom panel*, the time dependence of the relative concentrations of the three components shown in the middle panel as determined from the fitting of the spectra in the top panel. **C) Oxyferrous WT DHP B/Compound II:** *top panel*, stopped-flow UV–visible spectra of the double-mixing reaction of preformed Compound II with a 10-fold excess of 4-Br-*o*-cresol (619 scans over 10 s); inset: the single-wavelength (420 nm) dependence on time obtained from the raw spectra and its fit with a superposition of the calculated spectral components. *Middle panel*, the calculate spectra of the three reaction components derived from SVD analysis: Compound II (black), ferric DHP B (red) and the Fe–Br adduct (blue). *Bottom panel*, the time dependence of the relative concentrations of the three components shown in the middle panel as determined from the fitting of the spectra in the top panel.

Compound ES Reactivity: Formed in an aging line for 400 ms from an initial mixing step of ferric WT DHP B with 10 equiv H_2O_2 [38], Compound ES [418 (Soret), 546, 588 nm; black] was subsequently reacted with 10 equiv 4-Br-*o*-cresol at pH 7 (Fig. 6B), which led to reformation of ferric DHP B [406 (Soret), 505, 636 nm; t = 0.41 s, k_{obs} = 9.59 ± 0.07 s^{-1}; red]. At t = 10 s, the spectrum appeared as a mixture of the ferric enzyme and the same species observed in Compound I reactivity, namely the Fe–Br adduct [407 (Soret), 498, 605 nm, blue]. At longer times (500 s), full formation of the Fe-X adduct was confirmed, with no evidence of other species, i.e., Compound RH or oxyferrous DHP (data not shown). When this reaction was repeated with 4-F-*o*-cresol and 4-Cl-*o*-cresol, the observations of an initial reduction of Compound ES to the ferric enzyme, followed by formation of the Fe-X adduct, were qualitatively similar (Fig. S12). Substrate reduction of Compound ES to the ferric enzyme has been observed in past studies with halophenols [38], haloindoles [35], pyrrole [36], nitrophenols [25], and haloguaiacols [23]. However, unlike the product-driven reduction observed in those stopped-flow studies (by 2,6-chloroquinone [38], 5-Br-3-oxindole [35], and 2-methyoxybenzoquinone [23]) of the reformed ferric enzyme to the oxyferrous state, no formation of oxyferrous DHP B was observed here. We surmise that in the case of the halocresols, the putative reductant, 2-MeBq, was formed in too small of a concentration (Table S5) to drive the reduction of the ferric enzyme: employing 2-MeBq in benchtop studies showed it was only able to reduce ferric DHP to the oxyferrous state aerobically at or above 50 μM concentration (data not shown).

The reactivity of the remaining substrates with preformed Compound ES was also investigated in a manner identical to that described above for 4-Br-*o*-cresol. The time required for 10 equiv of each substrate to reduce Compound ES to the ferric state is listed in Table 5, and the representative reactions are shown in Figs. S12–S14. All substrates were found to convert Compound ES to the ferric enzyme, although the times varied > 50-fold (0.39–21.30 s): compared to *o*-cresol (3.99 s), the 4-R-*o*-cresol (R = F, Cl, Br, Me) substrates reduced Compound ES between 2 and 10-fold faster, whereas the more deactivated substrates (*m*-cresol, 4-Cl-*m*-cresol, and pentachlorophenol) were 2–5-fold slower.

Compound II Reactivity: Generated from an initial reaction of oxyferrous WT DHP B that was preincubated with 1 equiv of 2,4,6-trichlorophenol and mixed with H_2O_2 in an aging line for 2.75 s [44], preformed Compound II [421 (Soret), 546, 582 nm, black] was reacted with 10 equiv 4-Br-cresol (Fig. 6C). Similar to the findings noted for Compound ES, the Compound II intermediate was reduced to ferric DHP [405 (Soret), 506, and 638 nm; t = 1.66 s, k_{obs} = 5.34 ± 0.04 s^{-1}; red], and then formed a mixture with the Fe–Br adduct [407 (Soret), 498, 604 nm; blue, t = 10 s] at longer times. The reduction of Compound II to the ferric enzyme has been observed previously for 2,4,6-TCP [44], 5-Br-indole [35], pyrrole [36], 4-nitrophenol [25], and 4-Br-*o*-guaiacol [23], however further reduction of ferric DHP to oxyferrous enzyme was observed in these studies with the exception of 4-nitrophenol. Once again, we surmise that the lack of the product-driven formation here with 4-Br-*o*-cresol is attributable to the low concentration of the 2-MeBq product generated during catalytic turnover.

Oxyferrous Reactivity: In the absence of a substrate, oxyferrous DHP is unreactive towards H_2O_2 [44,75], exhibiting only a slight bleaching of the Soret band at short times, with long time scale conversion to Compound RH. Presumably, this is to prevent unwanted autoxidation of DHP in the absence of substrate. However, in the presence of virtually all known substrates, oxyferrous DHP exhibits a substrate-dependent activation by H_2O_2 [23,25,35,36,44,74,75]. To investigate if the cresols were also capable of activating oxyferrous DHP for oxidation by H_2O_2, a solution of oxyferrous WT DHP B preincubated with 10 equiv 4-Br-cresol [418 (Soret), 543, 578 nm; black, t = 0 s] was rapidly mixed with 10 equiv H_2O_2 (Fig. 7). The oxyferrous enzyme was initially oxidized to ferric DHP B [407 (Soret), 502, 609 nm; red, t = 8.7 s], and further converted to a stable species consistent with a mixture of ferric DHP and its Fe–Br adduct [408 (Soret), 606 nm; blue, t = 50 s]. In parallel studies employing 4-Br-*o*-guaiacol [23], the ferric enzyme similarly formed, however, reduction back to the oxyferrous enzyme was observed, which again highlights the lack of a product-driven reduction for 4-Br-*o*-cresol owing to the low amount of 2-MeBq formed during substrate turnover. No transiently formed Compound II species was observed here with 4-Br-*o*-cresol, which differs from past studies employing TCP [44], 5-Br-indole [35], and pyrrole [36] substrates that all proceeded through this ferryl species during activation of oxyferrous DHP. Regardless of whether Compound II was observed (halophenol, haloindole, pyrrole) or not (haloguaiacol, halocresol), the results here demonstrate that cresols are able to activate oxyferrous DHP for oxidation by H_2O_2.

The main observations from these stopped-flow studies were as follows: i) all reactions between preformed Compound I/ES/II and 4-Br-*o*-cresol yielded a DHP Fe–Br adduct, a species that has not been previously observed in catalytic studies with other halogenated substrates; ii) the H_2O_2-activated enzyme was reduced to ferric DHP by 4-Br-*o*-cresol, with the rate of reduction following the order: Compound I > Compound ES > Compound II, similar to previous studies with other classes of substrate [23,35,36,42]; iii) 4-Br-*o*-cresol was able to activate oxyferrous DHP B for reactivity with H_2O_2, however this occurred without the formation of an observable intermediate (i.e., Compound II); and iv) no product-driven reduction was observed for any reaction performed here, likely due to the low amount of 2-MeBq that forms from turnover, a result that again differs significantly from previous studies [23,35,38].

Proposed Peroxidase and Peroxygenase Mechanisms. Based on the labeling studies (*vide supra*), two oxidation mechanisms – peroxidase and peroxygenase – appear to be *concurrently* responsible for the oxidation of 4-Br-*o*-cresol to the 2-MeBq and catechol products, respectively. This is the first time that two concurrent mechanisms have been identified in the oxidation of a single substrate when catalyzed by DHP. In light of the results obtained above, and through modification of the previously established mechanisms for the DHP peroxidase [23,26,38,80] and peroxygenase [25,35,36] mechanisms, we propose the following two catalytic cycles for the H_2O_2-dependent oxidation of 4-X-*o*-cresol by ferric DHP B from *Amphitrite ornata*.

Peroxidase Mechanism – Scheme 1. Ferric DHP reacts initially with 1 equivalent H_2O_2 yielding a two-electron oxidized ferryl species, either as Compound I (step i-a) or Compound ES (step ii), both of which were shown to be reduced by 4-X-*o*-cresol. In the case of Compound I, a single two-electron oxidation of the substrate regenerates the resting ferric state and forms the 2-MeBq/Br^- products (step i-b), a reaction that has precedent with 4-Br-guaiacol [23] (note: two consecutive one-electron steps were ruled out owing to the absence of an observable Compound II species). However, in the case of Compound ES, the substrate is oxidized by consecutive one-electron processes (steps iii and iv) via a Compound II intermediate, regenerating the ferric state

Table 5
Summary of the Stopped-Flow UV–Visible Spectroscopic Data for the Reaction of Compound ES with EPA Pollutants and Related Substrates at pH 7.

Substrate	Compound ES → Ferric, time (s)	Observed Ferric species λ_{max} (nm)
o-cresol	3.99	409, 510, 634
m-cresol	9.30	407, 514, 638
p-cresol	4.34	409, 508, 631
4-Me-*o*-cresol	1.41	408, 506, 630
4-F-*o*-cresol	0.88	408, 506, 634
4-Cl-*o*-cresol	0.39	407, 506, 634
4-Br-*o*-cresol	0.41	406, 506, 636
4-NO_2-*o*-cresol[a]	n/a	n/a
4-Cl-*m*-cresol	19.80	407, 504, 625
pentachlorophenol	21.30	414, 539, 589

[a] n/a = not applicable, Compound RH formation was observed.

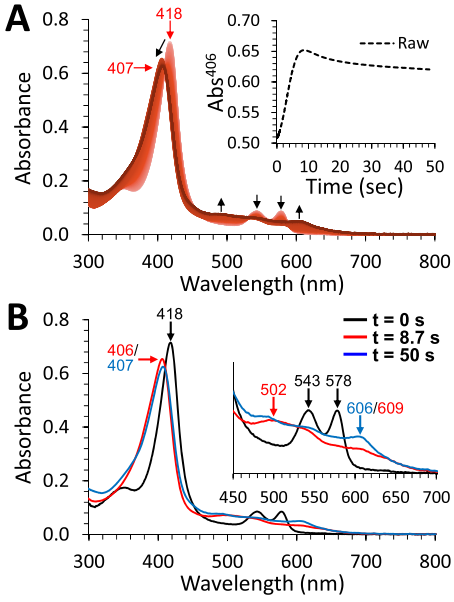

Fig. 7. Kinetic data obtained by optical spectroscopy for the reaction of oxyferrous DHP B with 4-Br-cresol and H_2O_2. A) stopped-flow UV–visible spectra of the single-mixing reaction of oxyferrous WT DHP B (10 μM) preincubated with a 10-fold excess of 4-Br-cresol and reacted with 10 equiv H_2O_2 at pH 7 (900 scans over 50 s); inset - the single wavelength (406 nm) dependence on time obtained from the raw spectra. B) the initially observed oxyferrous DHP species (black, t = 0 s), its reduction to the ferric enzyme (red, t = 8.7 s) and the formation of the Fe–Br adduct (blue, t = 50 s).

and forming 2-MeBq/Br^-. The 2-MeBq can form through oxidation of a 4-X-C• radical by activated DHP, or through disproportionation of two 4-X-C• radicals [83]. The observed higher-molecular weight oligomeric products likely arise from the reaction of these diffusible 4-X-C• radicals with 2-MeBq, with subsequent radical-radical coupling reactions yielding trimers, tetramers, etc. (Tables S1–S4). Although we did not observe a product-driven reduction of the ferric resting state during the pre-steady state stopped-flow experiments, 2-MeBq was able to reduce ferric DHP to the oxyferrous state at or above 50 μM concentration (step v), with oxyferrous DHP B capable of forming Compound II in the presence of substrate and H_2O_2 (step vi). For all reactions, formation of a DHP Fe–Br adduct was observed (step vii).

Peroxygenase Mechanism – Scheme 2. Starting from a common Compound I intermediate, itself formed from the reaction of ferric DHP with 1 equiv H_2O_2 (step i), two different pathways are proposed: electrophilic addition (step ii-a) or oxygen rebound (step ii-b). In the electrophilic addition pathway (step ii-a) [46], electrophilic addition of the ferryl oxygen to the substrate yields a tetrahedral-like σ-complex (step iii-a), with deprotonation of the substrate hydroxyl likely facilitated by the distal histidine (or other general base). Heterolytic cleavage of the Fe–O bond and protonation of the phenoxide (step iv-a), followed by keto-enol tautomerization (again possibly facilitated by the distal histidine) forms the catechol product and regenerates the resting ferric state (step v-a). While we propose that the distal histidine is playing the role of a general acid/base for the deprotonation/protonation events, we cannot rule out that a solvent water molecule or another amino acid residue is involved. In the oxygen rebound pathway [46], hydrogen atom abstraction yields a "caged" Compound II intermediate and a substrate radical [Fe^{IV}–OH •R] (step ii-b), which undergoes a classic rebound step (iii-b). As in the electrophilic addition pathway, keto-enol tautomerization (step iv-b) yields the desired catechol product.

Substituent Effects – "Substrate-Directed" Enzymatic Activity. The studies presented here provide strong evidence in support of our earlier supposition that it is possible to tune DHP activity [48,49], not through mutagenesis, directed evolution, or heme cofactor modification, but through selection of the substrate itself [23]. Specifically, that the properties of the substrate – its redox potential, binding/orientation within the distal pocket, distance to the heme, pK_a, and substituents – are all factors that determine which DHP activity (peroxygenase, peroxidase, oxidase, or oxygenase) leads to substrate oxidation. To this latter point of substituent effects, two sets of substrates provide an important observation vis-à-vis enzyme activity: i) 4-Br-phenol (inhibitor) [77], 4-Br-*o*-cresol (peroxygenase and peroxidase), and 4-Br-*o*-guaiacol (peroxidase) [23], and ii) 4-NO_2-phenol (peroxygenase) [25], 4-NO_2-*o*-cresol (peroxygenase and peroxidase), and 4-NO_2-*o*-guaiacol (peroxidase) [23]. In both sets, the progression of the *ortho* substituent of –H → -Me → -OMe shifts the activity of DHP from peroxygenase (or inhibition) to being an exclusively peroxidase-based mechanism. We surmise that the substituent factors into the discrimination between the peroxygenase and peroxidase activities through either i) steric effects – where the substrate binding distance is tuned between O-atom transfer,

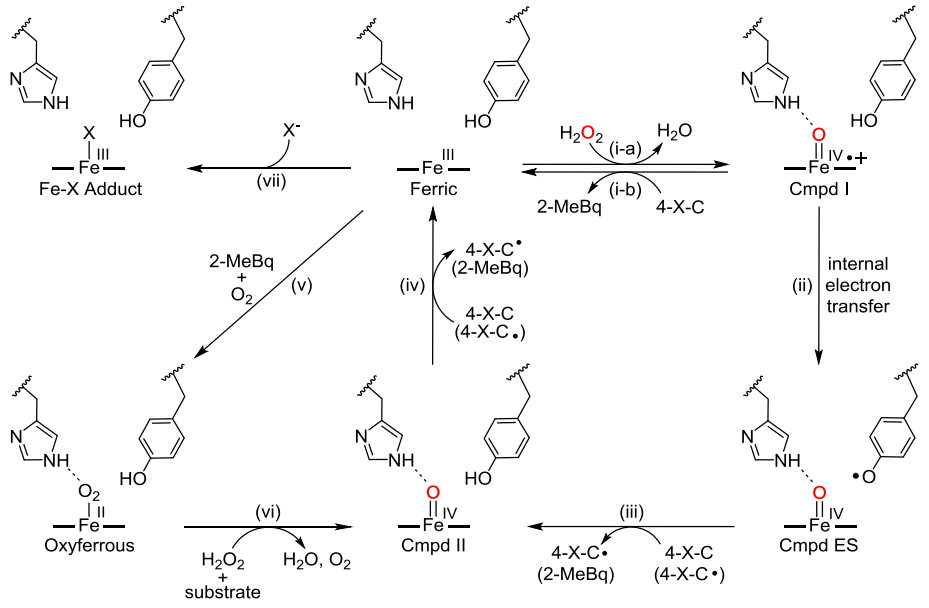

Scheme 1. Proposed Peroxidase Mechanism for the Oxidation of 4-X-*o*-Cresol (4-X-C) as Catalyzed by DHP B.

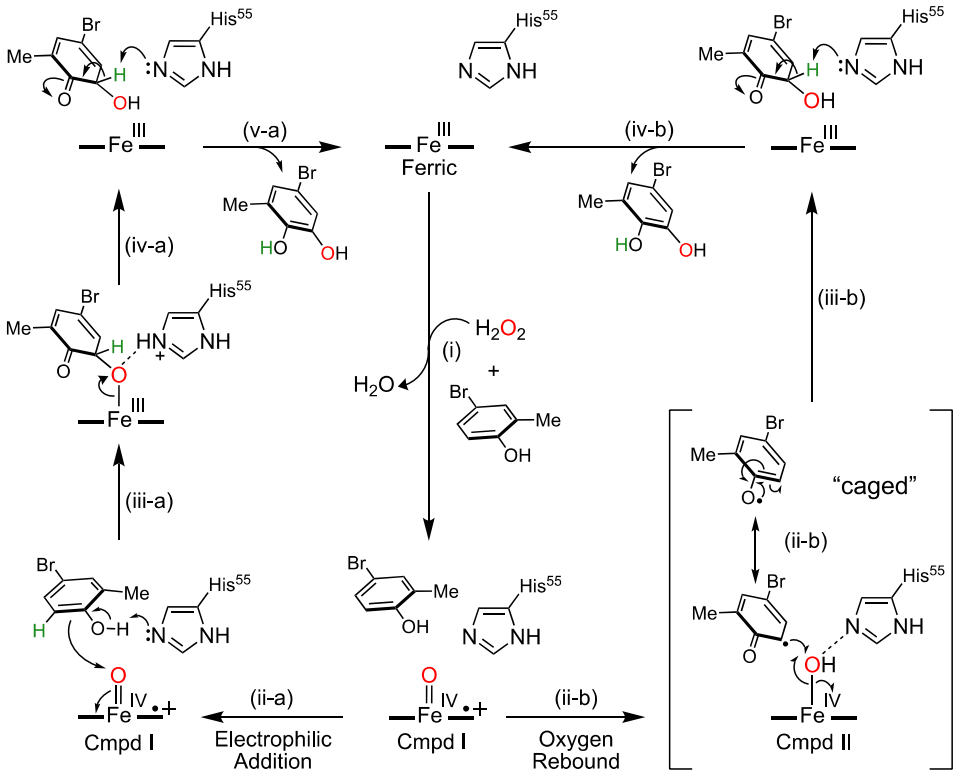

Scheme 2. Proposed Peroxygenase Mechanism for the Oxidation of 4-X-Cresol as Catalyzed by DHP B.

which necessitates a close interaction between the substrate and catalytic ferryl species (i.e., tetrahedral complex or 'caged' radical; Scheme 2) and electron transfer, which can occur over longer distances than atom transfer (Scheme 1), or ii) electronic effects – where resonance and/or inductive donating/withdrawing effects modulate electrophilic addition vs. (de)stabilization of a one-electron oxidized substrate radical. In the case of nitrophenols, the presence of a strong electron withdrawing group shifts the DHP activity towards O-atom transfer (peroxygenase) [25], whereas with guaiacols, the electron-donating group ensures oxidation via electron transfer (peroxidase), even for 4-NO_2-guaiacol [23]. For cresols, we observe here an intermediary effect, with the results of our crystallographic and binding studies clearly showing how subtle differences in size between the -OMe and -Me groups can lead to a significant change in how that substrate binds to DHP, an effect that can be used to 'tune' the activity of DHP, yielding concurrent peroxidase and peroxygenase mechanisms.

4. Conclusions

We have shown that dehaloperoxidase, a globin of marine origin, is able to catalyze the oxidation of cresol isomers (*o*-, *m*-, *p*-cresol), 4-R-*o*-cresol analogs (R = Me, NO_2, F, Cl, Br), and pentachlorophenol. Although there are extensive literature reports on the biodegradation of cresols and pentachlorophenol by several different microorganisms, dehaloperoxidase provides insight into the chemical reactivity of a globin of non-microbial origin that is able to degrade a wide range of cresol analogs. While the ability for dehaloperoxidase to function in this capacity is not surprising given that the degradation of *p*-cresol is widely known among peroxidases, what is unique to this multifunctional catalytic globin is that DHP is able to employ two concurrent mechanisms, peroxidase and peroxygenase, in the oxidation of a single cresol substrate. Our findings here contrast with previous work that established DHP as a multifunctional catalytic globin capable of either peroxidase or peroxygenase-based mechanisms for substrate oxidation, with no crossover between these two activities for a given class of substrate, i.e., halophenols, nitrocatechol, and haloguaiacols were all oxidized via peroxidase activity [23,25,38], and haloindoles, pyrrole, and nitrophenols were solely oxidized by a peroxygenase activity [25,35,36]. Here, we now show that substrates (e.g., cresols) cannot be simply or generally categorized as one that follows a specific DHP oxidation mechanism.

Having identified cresols as the fourth class of substrate, after haloindoles, nitrophenols and pyrroles, to undergo O-atom transfer, we are continuing to see the expanding substrate scope and versatility of dehaloperoxidase. The addition here of 4-Me-*o*-cresol, 4-Cl-*m*-cresol and pentachlorophenol increases the number of toxic phenolic compounds on the EPA Priority Pollutants list that are oxidized by DHP to 10 (out of 11) including phenol, 2-chlorophenol, 2,4-dichlorophenol, 2,4,6-trichlorophenol, 2-nitrophenol, 4-nitrophenol and 2,4-dinitrophenol, with only 2,4-dinitro-*o*-cresol having been shown to be unreactive. While the degradation of anthropogenic substrates *in vivo* remains to be elucidated, multifunctional globins such as DHP provide an unprecedented platform for deeply probing mechanistic questions related to the protein environment: by simply changing the substrate, we can investigate the unique set of protein-substrate interactions specific to each of the five different activities (oxygen-transport, peroxidase, peroxygenase, oxidase and oxygenase) of DHP, enabling us to pose questions related to multiple activities across the heme protein superfamily using just a single enzyme. More broadly, these studies demonstrate how the degradation pathways of EPA priority pollutants, as well as persistent organic pollutants generally, must go beyond microbial systems to include infaunal marine organisms in their environmental impact assessments.

Acknowledgments

This project was supported by the National Science Foundation (CHE-1609446). Mass spectrometry measurements were made in the Molecular Education, Technology, and Research Innovation Center (METRIC) at NC State University. X-ray diffraction data were collected

at Southeast Regional Collaborative Access Team (SER-CAT) ID22 and BM22 beamlines at the Advanced Photon Source, Argonne National Laboratory. Supporting institutions may be found at www.ser-cat.org/members.html. Use of the Advanced Photon Source was supported by the U. S. Department of Energy, Office of Science, Office of Basic Energy Sciences, under Contract No. W-31-109-Eng-38. We would like to thank Dr. Edwin Pozharski for helpful discussions in crystallographic data processing, and we would like to thank Dr. Paul Swartz for his assistance in data collection at the SERCAT beamlines.

Appendix A. Supplementary data

Supplementary data to this article can be found online at https://doi.org/10.1016/j.abb.2019.108079.

References

[1] Title 40 - Protection of Environment, Code of Federal Regulations, Section 423, Appendix A, U.S. Environmental Protection Agency, Washington, D.C., 2013.
[2] Title 15 U.S. Code Chapter 53 - Toxic Substances Control Act, (1976).
[3] B.M. Adedigba, K.T. Semple, Chapter 15 - bioavailability of persistent organic pollutants in soils: concept, analytical tools, and application in the risk assessment, in: Y.Z. Eddy (Ed.), Comprehensive Analytical Chemistry, Elsevier, 2015, pp. 493–512.
[4] R.P. Schwarzenbach, T. Egli, T.B. Hofstetter, U.v. Gunten, B. Wehrli, Global water pollution and human health, Annu. Rev. Environ. Resour. 35 (2010) 109–136.
[5] M.l. Farré, S. Pérez, L. Kantiani, D. Barceló, Fate and toxicity of emerging pollutants, their metabolites and transformation products in the aquatic environment, Trends Anal. Chem. 27 (2008) 991–1007.
[6] W. Duan, F. Meng, H. Cui, Y. Lin, G. Wang, J. Wu, Ecotoxicity of phenol and cresols to aquatic organisms: a review, Ecotoxicol. Environ. Saf. 157 (2018) 441–456.
[7] Q. Fang, X. Shi, L. Zhang, Q. Wang, X. Wang, Y. Guo, B. Zhou, Effect of titanium dioxide nanoparticles on the bioavailability, metabolism, and toxicity of pentachlorophenol in zebrafish larvae, J. Hazard Mater. 283 (2015) 897–904.
[8] M. Hofrichter, F. Bublitz, W. Fritsche, Cometabolic degradation of o-cresol and 2,6-dimethylphenol by Penicillium frequentans Bi 7/2, J. Basic Microbiol. 35 (1995) 303–313.
[9] R.K. Singh, S. Kumar, S. Kumar, A. Kumar, Biodegradation kinetic studies for the removal of p-cresol from wastewater using Gliomastix indicus MTCC 3869, Biochem. Eng. J. 40 (2008) 293–303.
[10] S. Bera, H. Kauser, K. Mohanty, Optimization of p-cresol biodegradation using novel bacterial strains isolated from petroleum hydrocarbon fallout, J. Water Process Eng. 31 (2019) 100842.
[11] R. Surkatti, S. Al-Zuhair, Effect of cresols treatment by microalgae on the cells' composition, J. Water Process Eng. 26 (2018) 250–256.
[12] R. Carmichael, P.M. Fedorak, M.A. Pickard, Oxidation of phenols by chloroperoxidase, Biotechnol. Lett. 7 (1985) 289–294.
[13] H. Wariishi, H.B. Dunford, I.D. MacDonald, M.H. Gold, Manganese peroxidase from the lignin-degrading basidiomycete Phanerochaete chrysosporium. Transient state kinetics and reaction mechanism, J. Biol. Chem. 264 (1989) 3335–3340.
[14] V.A. Edalli, S.I. Mulla, S.A.M.A.S. Eqani, G.D. Mahadevan, R. Sharma, Y. Shouche, C.M. Kamanavalli, Evaluation of p-cresol degradation with polyphenol oxidase (PPO) immobilized in various matrices, 3 Biotech 6 (2016) 229.
[15] A. Çelik, P.M. Cullis, E. Lloyd Raven, Catalytic oxidation of p-cresol by ascorbate peroxidase, Arch. Biochem. Biophys. 373 (2000) 175–181.
[16] M.D. Aitken, I.J. Massey, T. Chen, P.E. Heck, Characterization of reaction products from the enzyme catalyzed oxidation of phenolic pollutants, Water Res. 28 (1994) 1879–1889.
[17] M.A. Bhat, C.S. Vaidyanathan, Microbial degradation of halogenated aromatics, in: V.P. Singh (Ed.), Progress in Industrial Microbiology, Elsevier, 1995, pp. 125–156.
[18] R.P. Hayes, T.W. Moural, K.M. Lewis, D. Onofrei, L. Xun, C. Kang, Structures of the inducer-binding domain of pentachlorophenol-degrading gene regulator PcpR from Sphingobium chlorophenolicum, Int. J. Mol. Sci. 15 (2014) 20736–20752.
[19] J.E. West, S.M. O'Neill, G.M. Ylitalo, Time trends of persistent organic pollutants in benthic and pelagic indicator fishes from puget sound, Washington, USA, Arch. Environ. Contam. Toxicol. 73 (2017) 207–229.
[20] K. Magnusson, R. Ekelund, R. Grabic, P.A. Bergqvist, Bioaccumulation of PCB congeners in marine benthic infauna, Mar. Environ. Res. 61 (2006) 379–395.
[21] A.S. Szczybelski, M.J. van den Heuvel-Greve, T. Kampen, C. Wang, N.W. van den Brink, A.A. Koelmans, Bioaccumulation of polycyclic aromatic hydrocarbons, polychlorinated biphenyls and hexachlorobenzene by three Arctic benthic species from Kongsfjorden (Svalbard, Norway), Mar. Pollut. Bull. 112 (2016) 65–74.
[22] I. Vieweg, H. Hop, T. Brey, S. Huber, W.G. Ambrose, W.L. Locke V, G.W. Gabrielsen, Persistent organic pollutants in four bivalve species from Svalbard waters, Environ. Pollut. 161 (2012) 134–142.
[23] A.H. McGuire, L.M. Carey, V. de Serrano, S. Dali, R.A. Ghiladi, Peroxidase versus peroxygenase activity: substrate substituent effects as modulators of enzyme function in the multifunctional catalytic globin dehaloperoxidase, Biochemistry 57 (2018) 4455–4468.
[24] N.L. McCombs, T. Moreno-Chicano, L.M. Carey, S. Franzen, M.A. Hough, R.A. Ghiladi, Interaction of azole-based environmental pollutants with the coelomic hemoglobin from amphitrite ornata: a molecular basis for toxicity, Biochemistry 56 (2017) 2294–2303.
[25] N.L. McCombs, J. D'Antonio, D.A. Barrios, L.M. Carey, R.A. Ghiladi, Nonmicrobial nitrophenol degradation via peroxygenase activity of dehaloperoxidase-hemoglobin from *Amphitrite ornata*, Biochemistry 55 (2016) 2465–2478.
[26] S. Franzen, R.A. Ghiladi, L. Lebioda, J. Dawson, Chapter 10 Multi-Functional Hemoglobin Dehaloperoxidases, Heme Peroxidases, The Royal Society of Chemistry, 2016, pp. 218–244.
[27] E. Zhang, Y.P. Chen, M.P. Roach, D.E. Lincoln, C.R. Lovell, S.A. Woodin, J.H. Dawson, L. Lebioda, Crystallization and initial spectroscopic characterization of the heme-containing dehaloperoxidase from the marine polychaete *Amphitrite ornata*, Acta Crystallogr. Sect. D Biol. Crystallogr. 52 (1996) 1191–1193.
[28] L. Lebioda, M.W. LaCount, E. Zhang, Y.P. Chen, K. Han, M.M. Whitton, D.E. Lincoln, S.A. Woodin, An enzymatic globin from a marine worm, Nature 401 (1999) 445.
[29] M.W. LaCount, E. Zhang, Y.P. Chen, K. Han, M.M. Whitton, D.E. Lincoln, S.A. Woodin, L. Lebioda, The crystal structure and amino acid sequence of dehaloperoxidase from *Amphitrite ornata* indicate common ancestry with globins, J. Biol. Chem. 275 (2000) 18712–18716.
[30] L. Pollock, A Practical Guide to the Marine Animals of Northeastern North America, Rutgers University Press, New Brunswick, 1998.
[31] G.W. Gribble, Naturally Occurring Organohalogen Compounds - A Comprehensive Update, Springer, Vienna, 2010.
[32] Y.P. Chen, S.A. Woodin, D.E. Lincoln, C.R. Lovell, An unusual dehalogenating peroxidase from the marine terebellid polychaete *Amphitrite ornata*, J. Biol. Chem. 271 (1996) 4609–4612.
[33] R.E. Weber, C. Mangum, H. Steinman, C. Bonaventura, B. Sullivan, J. Bonaventura, Hemoglobins of two terebellid polychaetes: *Enoplobranchus sanguineus* and *Amphitrite ornata*, Comp. Biochem. Physiol. A Comp. Physiol. 56 (1977) 179–187.
[34] S. Sun, M. Sono, C. Wang, J. Du, L. Lebioda, J.H. Dawson, Influence of heme environment structure on dioxygen affinity for the dual function *Amphitrite ornata* hemoglobin/dehaloperoxidase. Insights into the evolutional structure–function adaptations, Arch. Biochem. Biophys. 545 (2014) 108–115.
[35] D.A. Barrios, J. D'Antonio, N.L. McCombs, J. Zhao, S. Franzen, A.C. Schmidt, L.A. Sombers, R.A. Ghiladi, Peroxygenase and oxidase activities of dehaloperoxidase-hemoglobin from *Amphitrite ornata*, J. Am. Chem. Soc. 136 (2014) 7914–7925.
[36] N.L. McCombs, T. Smirnova, R.A. Ghiladi, Oxidation of pyrrole by dehaloperoxidase-hemoglobin: chemoenzymatic synthesis of pyrrolin-2-ones, Catal. Sci. Technol. 7 (2017) 3104–3118.
[37] J. Feducia, R. Dumarieh, L.B. Gilvey, T. Smirnova, S. Franzen, R.A. Ghiladi, Characterization of dehaloperoxidase compound ES and its reactivity with trihalophenols, Biochemistry 48 (2009) 995–1005.
[38] J. D'Antonio, E.L. D'Antonio, M.K. Thompson, E.F. Bowden, S. Franzen, T. Smirnova, R.A. Ghiladi, Spectroscopic and mechanistic investigations of dehaloperoxidase B from *Amphitrite ornata*, Biochemistry 49 (2010) 6600–6616.
[39] J. Du, X. Huang, S. Sun, C. Wang, L. Lebioda, J.H. Dawson, *Amphitrite ornata* dehaloperoxidase (DHP): investigations of structural factors that influence the mechanism of halophenol dehalogenation using “Peroxidase-like” myoglobin mutants and “Myoglobin-like” DHP mutants, Biochemistry 50 (2011) 8172–8180.
[40] R.L. Osborne, M.K. Coggins, G.M. Raner, M. Walla, J.H. Dawson, The mechanism of oxidative halophenol dehalogenation by *Amphitrite ornata* dehaloperoxidase is initiated by H_2O_2 binding and involves two consecutive one-electron steps: role of ferryl intermediates, Biochemistry 48 (2009) 4231–4238.
[41] (Manuscript in preparation).
[42] R. Dumarieh, J. D'Antonio, A. Deliz-Liang, T. Smirnova, D.A. Svistunenko, R.A. Ghiladi, Tyrosyl Radicals in Dehaloperoxidase: how nature deals with evolving an oxygen-binding globin to a biologically relevant peroxidase, J. Biol. Chem. 288 (2013) 33470–33482.
[43] R. Davydov, R.L. Osborne, M. Shanmugam, J. Du, J.H. Dawson, B.M. Hoffman, Probing the oxyferrous and catalytically active ferryl states of *Amphitrite ornata* dehaloperoxidase by cryoreduction and EPR/ENDOR spectroscopy. Detection of compound I, J. Am. Chem. Soc. 132 (2010) 14995–15004.
[44] J. D'Antonio, R.A. Ghiladi, Reactivity of deoxy- and oxyferrous dehaloperoxidase B from *Amphitrite ornata*: identification of compound II and its ferrous-hydroperoxide precursor, Biochemistry 50 (2011) 5999–6011.
[45] H.B. Dunford, Chapter 5 Heme Peroxidase Kinetics, Heme Peroxidases, The Royal Society of Chemistry, 2016, pp. 99–112.
[46] X. Huang, J.T. Groves, Oxygen activation and radical transformations in heme proteins and metalloporphyrins, Chem. Rev. 118 (2018) 2491–2553.
[47] P.R. Ortiz de Montellano, Cytochrome P450: Structure, Mechanism, and Biochemistry, Springer International Publishing, 2015, p. 912.
[48] L.M. Carey, K.B. Kim, N.L. McCombs, P. Swartz, C. Kim, R.A. Ghiladi, Selective tuning of activity in a multifunctional enzyme as revealed in the F21W mutant of dehaloperoxidase B from *Amphitrite ornata*, J. Biol. Inorg. Chem. 23 (2018) 209–219.
[49] L.M. Carey, R. Gavenko, D.A. Svistunenko, R.A. Ghiladi, How nature tunes isoenzyme activity in the multifunctional catalytic globin dehaloperoxidase from *Amphitrite ornata*, Biochim. Biophys. Acta 1866 (2018) 230–241.
[50] V. de Serrano, J. D'Antonio, S. Franzen, R.A. Ghiladi, Structure of dehaloperoxidase B at 1.58 A resolution and structural characterization of the AB dimer from *Amphitrite ornata*, Acta Crystallogr. D66 (2010) 529–538.
[51] A. Castro-Forero, D. Jiménez, J. López-Garriga, M. Torres-Lugo, Immobilization of myoglobin from horse skeletal muscle in hydrophilic polymer networks, J. Appl. Polym. Sci. 107 (2008) 881–890.
[52] V.N. Goral, A.D. Ryabov, Reactivity of the horseradish peroxidase compounds I and

II toward organometallic substrates. A stopped-flow kinetic study of oxidation of ferrocenes, IUBMB Life 45 (1998) 61–71.
[53] M. Guazzaroni, C. Crestini, R. Saladino, Layer-by-Layer coated tyrosinase: an efficient and selective synthesis of catechols, Bioorg. Med. Chem. 20 (2012) 157–166.
[54] J.N. Rodríguez-López, L.G. Fenoll, M.a.J. Peñalver, P.A. García-Ruiz, R. Varón, F. Martínez-Ortíz, F. García-Cánovas, J. Tudela, Tyrosinase action on monophenols: evidence for direct enzymatic release of o-diphenol, BBA-Protein Struct. Mol. Enzym. 1548 (2001) 238–256.
[55] C.C. Sweeley, R. Bentley, M. Makita, W.W. Wells, Gas-liquid chromatography of trimethylsilyl derivatives of sugars and related Substances, J. Am. Chem. Soc. 85 (1963) 2497–2507.
[56] P. Chenprakhon, J. Sucharitakul, B. Panijpan, P. Chaiyen, Measuring binding affinity of protein-ligand interaction using spectrophotometry: binding of neutral red to riboflavin-binding protein, J. Chem. Educ. 87 (2010) 829–831.
[57] Z. Otwinowski, W. Minor, Processing of X-ray diffraction data collected in oscillation mode, in: C.W. Carter Jr, R.M. Sweet (Eds.), Methods in Enzymology, Academic Press, New York, 1997, pp. 307–326.
[58] A.J. McCoy, R.W. Grosse-Kunstleve, P.D. Adams, M.D. Winn, L.C. Storoni, R.J. Read, Phaser crystallographic software, J. Appl. Crystallogr. 40 (2007) 658–674.
[59] P. Emsley, B. Lohkamp, W.G. Scott, K. Cowtan, Features and development of coot, Acta Crystallogr. D66 (2010) 486–501.
[60] G.N. Murshudov, A.A. Vagin, E.J. Dodson, Refinement of macromolecular structures by the maximum-likelihood method, Acta Crystallogr. D53 (1997) 240–255.
[61] Collaborative Computational Project, The CCP4 suite: programs for protein crystallography, Acta Crystallogr. D50 (1994) 760–763.
[62] P.D. Adams, P.V. Afonine, G. Bunkoczi, V.B. Chen, I.W. Davis, N. Echols, J.J. Headd, L.W. Hung, G.J. Kapral, R.W. Grosse-Kunstleve, A.J. McCoy, N.W. Moriarty, R. Oeffner, R.J. Read, D.C. Richardson, J.S. Richardson, T.C. Terwilliger, P.H. Zwart, PHENIX: a comprehensive Python-based system for macromolecular structure solution, Acta Crystallogr. D66 (2010) 213–221.
[63] P.V. Afonine, R.W. Grosse-Kunstleve, N. Echols, J.J. Headd, N.W. Moriarty, M. Mustyakimov, T.C. Terwilliger, A. Urzhumtsev, P.H. Zwart, P.D. Adams, Towards automated crystallographic structure refinement with phenix.refine, Acta Crystallogr. D68 (2012) 352–367.
[64] V.B. Chen, W.B. Arendall 3rd, J.J. Headd, D.A. Keedy, R.M. Immormino, G.J. Kapral, L.W. Murray, J.S. Richardson, D.C. Richardson, MolProbity: all-atom structure validation for macromolecular crystallography, Acta Crystallogr. Sect. D Biol. Crystallogr. 66 (2010) 12–21.
[65] R.P. Joosten, F. Long, G.N. Murshudov, A. Perrakis, The PDB_REDO server for macromolecular structure model optimization, IUCrJ 1 (2014) 213–220.
[66] CRC Handbook of Chemistry and Physics, 99th ed., CRC Press, Boca Raton, Fl.
[67] Ionisation constants of organic acids in aqueous solution, in: E.P. Serjeant, B. Dempsey (Eds.), International Union of Pure Applied Chemistry, Pergamon Press New York, NY, 1979.
[68] A.J. Cessna, R. Grover, Spectrophotometric determination of dissociation constants of selected acidic herbicides, J. Agric. Food Chem. 26 (1978) 289–292.
[69] R.P. Schwarzenbach, R. Stierli, B.R. Folsom, J. Zeyer, Compound properties relevant for assessing the environmental partitioning of nitrophenols, Environ. Sci. Technol. 22 (1988) 83–92.
[70] M.K. Thompson, M.F. Davis, V. de Serrano, F.P. Nicoletti, B.D. Howes, G. Smulevich, S. Franzen, Internal binding of halogenated phenols in dehaloperoxidase-hemoglobin inhibits peroxidase function, Biophys. J. 99 (2010) 1586–1595.
[71] M.F. Davis, H. Gracz, F.A. Vendeix, V. de Serrano, A. Somasundaram, S.M. Decatur, S. Franzen, Different modes of binding of mono-, di-, and trihalogenated phenols to the hemoglobin dehaloperoxidase from *Amphitrite ornata*, Biochemistry 48 (2009) 2164–2172.
[72] C. Wang, L.L. Lovelace, S. Sun, J.H. Dawson, L. Lebioda, Complexes of dual-function hemoglobin/dehaloperoxidase with substrate 2,4,6-trichlorophenol are inhibitory and indicate binding of halophenol to compound I, Biochemistry 52 (2013) 6203–6210.
[73] K. Nienhaus, P. Deng, J. Belyea, S. Franzen, G.U. Nienhaus, Spectroscopic study of substrate binding to the carbonmonoxy form of dehaloperoxidase from *Amphitrite ornata*, J. Phys. Chem. B 110 (2006) 13264–13276.
[74] S. Sun, M. Sono, J. Du, J.H. Dawson, Evidence of the direct involvement of the substrate TCP radical in functional switching from oxyferrous O_2 carrier to ferric peroxidase in the dual-function hemoglobin/dehaloperoxidase from *Amphitrite ornata*, Biochemistry 53 (2014) 4956–4969.
[75] J. Du, M. Sono, J.H. Dawson, Functional switching of *Amphitrite ornata* dehaloperoxidase from O_2-binding globin to peroxidase enzyme facilitated by halophenol substrate and H_2O_2, Biochemistry 49 (2010) 6064–6069.
[76] J. Zhao, J. Moretto, P. Le, S. Franzen, Measurement of internal substrate binding in dehaloperoxidase-hemoglobin by competition with the heme-fluoride binding equilibrium, J. Phys. Chem. B 119 (2015) 2827–2838.
[77] J. Zhao, S. Franzen, Kinetic study of the inhibition mechanism of dehaloperoxidase-hemoglobin a by 4-bromophenol, J. Phys. Chem. B 117 (2013) 8301–8309.
[78] J. Zhao, V. de Serrano, P. Le, S. Franzen, Structural and kinetic study of an internal substrate binding site in dehaloperoxidase-hemoglobin A from *Amphitrite ornata*, Biochemistry 52 (2013) 2427–2439.
[79] E.L. D'Antonio, J. D'Antonio, V. de Serrano, H. Gracz, M.K. Thompson, R.A. Ghiladi, E.F. Bowden, S. Franzen, Functional consequences of the creation of an Asp-His-Fe triad in a 3/3 globin, Biochemistry 50 (2011) 9664–9680.
[80] S. Franzen, M.K. Thompson, R.A. Ghiladi, The dehaloperoxidase paradox, Biochim. Biophys. Acta 1824 (2012) 578–588.
[81] V. de Serrano, S. Franzen, Structural evidence for stabilization of inhibitor binding by a protein cavity in the dehaloperoxidase-hemoglobin from *Amphitrite ornata*, Biopolymers 98 (2012) 27–35.
[82] M.K. Thompson, S. Franzen, R.A. Ghiladi, B.J. Reeder, D.A. Svistunenko, Compound ES of dehaloperoxidase decays via two alternative pathways depending on the conformation of the distal histidine, J. Am. Chem. Soc. 132 (2010) 17501–17510.
[83] S. Franzen, K. Sasan, B.E. Sturgeon, B.J. Lyon, B.J. Battenburg, H. Gracz, R. Dumariah, R.A. Ghiladi, Nonphotochemical base-catalyzed hydroxylation of 2,6-dichloroquinone by H_2O_2 occurs by a radical mechanism, J. Phys. Chem. B 116 (2012) 1666–1676.